

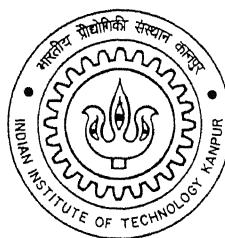
401062

Effect of Thermomechanical Processing on the Fatigue and Tensile Behavior of the Forging Grade Microalloyed Steels

By

Sqn Ldr Prem Singh

TH
MME/2002/M
Si 64e



Department of Materials and Metallurgical Engineering

INDIAN INSTITUTE OF TECHNOLOGY KANPUR

January, 2002

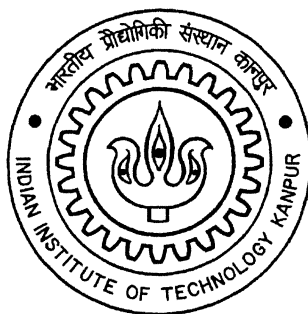
Effect of Thermomechanical Processing on the Fatigue and Tensile Behavior of the Forging Grade Microalloyed Steels

A Thesis
Submitted by

Sqn Ldr Prem Singh

For the award of the degree of

Master of Technology



**Department of Materials and Metallurgical Engineering
Indian Institute of Technology
Kanpur**

Jan 2002

- 5 MAR 2002 / MME

पुरुषोत्तम का गीताप क्षेत्र पुस्तकालय

भारतीय प्रौद्योगिकी संस्थान कानपुर

अवधि क्र० A 137952.....



A137952

Effect of Thermomechanical Processing on the Fatigue and Tensile Behavior of the Forging Grade Microalloyed Steels

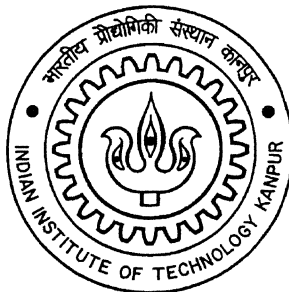
A Thesis Submitted .

**In Partial Fulfillment of the Requirements
for the Degree of**

Master of Technology

by

Sqn Ldr Prem Singh

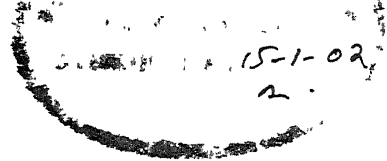


to the

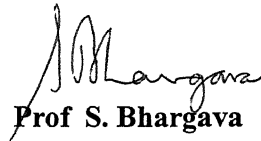
**Department of Materials and Metallurgical Engineering
Indian Institute of Technology
Kanpur**

Jan 2002

certificate



This is to certify that the thesis entitled **“Effect of Thermomechanical Processing on the Fatigue and Tensile Behavior of the Forging Grade Microalloyed Steels”** submitted by Sqn Ldr Prem Singh (Roll No. Y010624) to the Indian Institute of Technology Kanpur for the award of Master of Technology is a bona fide record of research work carried out under my supervision. The contents of this, in full or in parts, have not been submitted to any other institute or university for the award of any degree or diploma.

A handwritten signature in black ink, appearing to read "S. Bhargava".

Prof S. Bhargava

Research Guide

Department of Materials and

Metallurgical Engineering

Indian Institute of Technology

Kanpur-208016, India

Kanpur

Date: 14/01/02

abstract

Microalloyed (MA) and control processed low carbon and medium carbon ferrite-pearlite steels are increasingly used in automotive and structural applications in place of quenched and tempered (Q & T) steels. This thesis deals with the room temperature tensile properties and low- and high-cycle fatigue behavior of a medium carbon microalloyed steel (38MnSiVS5) in different microstructural conditions obtained by thermomechanical processing schedules. Hot rolled blooms of 38MnSiVS5 steel of 65 mm RCS were reduced to 25.4 mm diameter bars by machining and were soaked at 1200°C for 1 hour to be subsequently controlled hot rolled to 17 mm diameter bars in 6-8 passes at the finishing temperatures of 800°C, 900°C and 1000°C. Hot rolled bars were subsequently air cooled to room temperature. Microstructures, as analyzed by optical and scanning electron microscopy, after three different thermomechanical processing i.e. TMP1 (finish rolling temperature of 800°C), TMP2 (finish rolling temperature of 900°C) and TMP3 (finish rolling temperature of 1000°C) comprised of polygonal ferrite/fine pearlite (PF/FP), polygonal ferrite/medium pearlite (PF/MP) and polygonal ferrite/coarse pearlite (PF/CP) respectively. In addition, volume fractions of free ferrite and pearlite as well as ferrite grain size were found to be different in the steel processed through the above TMP schedules.

Tensile properties of the steel after TMP1, TMP2 and TMP3 were found to be superior to that of the as-received material. Among the three TMP schedules, 0.2% yield strength, hardness and the UTS were found to be highest for the material processed through TMP1. ‡

Cyclic stress response as observed in the cyclic stress – strain curves showed that all the structures underwent cyclic hardening at high strain amplitudes ($>0.6\%$) and cyclic softening followed by steady state behaviour at low strain amplitudes ($\leq 0.6\%$). However, steel processed through TMP3 showed steady state behaviour for more number of cycles as compared to steel processed through TMP1 and TMP2 for the same amount of strain amplitudes. Further, the value of the cyclic strain hardening exponent was also found to be highest for TMP3 as compared to TMP1 and TMP2. The low cycle fatigue life at low and high plastic strain amplitudes respectively was found to be 35% to 60% more for the TMP3 as compared to TMP1 and TMP2. As

revealed by fractography the mode of State II crack propagation was found to be by void growth and coalescence for all the TMP conditions. Moreover, the fractured surfaces of all conditions showed fatigue striations typical of pearlitic microstructures. The stress-life plots in the high cycle fatigue regime were obtained for TMP1 and TMP2 conditions. The fatigue limit for PF/FP and PF/MP microstructures was found to be 462 MPa and 437 MPa respectively. The low as well as high cycle fatigue test results, as obtained in the present study, showed that the fatigue behavior of medium carbon microalloyed 38MnSiVS5 steel can be significantly varied by its thermomechanical processing. It is, therefore, concluded that the thermomechanical processing schedule should be given due importance for properly optimizing the mechanical properties of medium carbon microalloyed 38MnSiVS5 steel.

acknowledgements

I would like to express my deep sense of gratitude and sincere thanks to **Prof. K.A. Padmanabhan** and **Prof. S.Bhargava** ,my research guides ,for providing me an opportunity to initiate myself in the very interesting area of fatigue of steels. I would also like to thank them for helpful guidance and constant encouragement despite their extremely busy schedule.

I am thankful to Indian Air Force, my parent organization, for sponsoring my M.Tech. course in Materials and Metallurgical Engineering from IIT Kanpur.

I want to convey my thanks to **Mr. B.K.Jain** ,lab in-charge Materials Testing Lab ,for his invaluable help in carrying out the fatigue experiments, often beyond the call of duty.His assistance in the general course of this investigation is also deeply acknowledged.

I wish to express my profound thanks to **Prof. S.Sangal** for his help in getting the project started and taking out time to visit to field gun factory with me for the forging job. He imparted a lot of his experience in the conduct of the experiments. Also his help in image analysis is acknowledged.

I am thankful to **Dr. O.N.Mohanty** ,Director (R&D) TISCO,Jamshedpur for supplying the material for this study. I also wish to thank Department of Science and Technology, Government of India for funding this project.

I thank **Prof. V.Bansal** and **Prof. B. Deo** for their guidance, encouragement and valuable tips on the failure analysis and data analysis respectively.

I express my sincere thanks to **Dr. Gouthama** for his keen interest in my progress, for his constant encouragement and support. His help in analyzing Optical, SEM micrographs and Fractography is also acknowledged.

I am thankful to **Mr.S.P.Rai** ,**Mr C.L.Sachan** and all the staff of Metallurgical Engineering Lab for their help in Thermo Mechanical processing of the samples.

I wish to thank **Mr. V.K.Srivastava** , **Mr. Sharma**, **Mr. Anil Kumar** ,**Mr. Pramod Kumar** of Central Workshop for machining of the Fatigue and Tensile samples and other jobs as were required.

I wish to thank **Dr. M.N. Mungole** for his help in preparation of metallographic samples & development of negatives.

I am grateful to **Mr Agnihotri & Mr Singh** for their help in carrying out SEM & EPMA investigations . I also thank **Mr. Sharma** for development of SEM negatives.

I am thankful to **Mr. Brejendra Singh (Kumar Ji)** for his help in the repair of the furnace.

I thank **Lt. S. Chhabra**, my fellow research scholar, for his help in Image Analyser .

I have great pleasure in thanking **Mr. S.Sankaran** , PhD. scholar, and **Mr S.John,Mr. G.J.Sunil ,Mr. Rajil, Mr. S.Poddar,Mr. Satish Gotam , Mr. V. Kaushik, Miss Madhuri & Mrs Indrani Chakraborty**,my fellow research scholars, for providing a jovial atmosphere ,valuable suggestions and simulating discussions.

I also wish to thank my colleague defence officers ,my fellow research scholars,**Sqn Ldr S Sareen, Sqn Ldr PA Patil ,Sqn Ldr M Naik,Flt Lt Prasad,Col Khanna,Maj Rajat,Maj Mohan,Major Vaidya** and others for giving me company during my stay & their willingness to help whenever asked.

I want to express my thanks to my family members my wife **Meenali**, daughter **Divya**, son **Shreyas** and my Mother **Smt Shanti Devi** for showing the patience and giving me moral support during the long working hours that I had while working on this project.

Lastly, I would like to thank all the faculty members, staff and students of department of **Materials and Metallurgical Engineering** for a wonderful learning experience that I had at IIT Kanpur.

Sqn Ldr Prem Singh

contents

Certificate	ii
Abstract	iii
Acknowledgements	v
Contents	vii
List of Figures	xi
List of Tables	xiv
1. Introduction	
1.1 Definition	2
1.2 Industrial Significance	2
1.3 Design against Fatigue	3
2. Literature Review	
2.1 Introduction	5
2.1.1 The Rationale of Microalloyed High Strength Steels	5
2.1.2 Application of HSLA Steels	8
2.2 Growth of Microalloyed Steels	9
2.2.1 Grain Refined Steels	9
2.2.2 Precipitation Strengthening	10
2.2.3 Development of Controlled Rolling	10
2.2.4 Development of Controlled Cooling	10
2.2.5 Low Carbon Ferrite-Pearlite Steels	11
2.2.6 Acicular Ferrite Steels	11

2.2.7	Dual Phase Steels	11
2.2.8	Inclusion Shape Control	11
2.3	Classifications	12
2.3.1	Microalloyed Ferrite-Pearlite Steels	13
2.4	Role of Microalloying Elements	14
2.4.1	Solubility Effects	15
2.4.2	Grain Refinement	15
2.4.3	Precipitation Strengthening	16
2.4.4	Alloying Elements	16
2.5	Steelmaking	17
2.6	Thermomechanical Treatments for Sheets ,Strips & Plates	18
2.6.1	Thermomechanical Working & Controlled Rolling	18
2.6.1.1	Conventional Low Temp Rolling	19
2.6.1.2	Recrystallization Controlled Rolling	19
2.6.2	Controlled Cooling	20
2.7	HSLA Forgings	21
2.7.1	Metallurgical Effects	21
2.7.2	Development of HSLA Forging Steels	21
2.7.2.1	First Generation MA Forging Steels	22
2.7.2.2	Second Generation MA Forging Steels	22
2.7.2.3	Third Generation MA Forging Steels	22
2.8	Mechanical Properties of HSLA Steels	23
2.8.1	Monotonic Loading Behavior	23
2.8.2	Cyclic Response	23
3.	Scope of The Present Investigation	
3.1	Material for the Present Investigation	24
3.2	Objective and Scope of the Present Investigation	24
4.	Experimental Procedure	
4.1	Starting Material	26
4.1.1	Chemistry	26

4.1.2	Microstructure	26
4.2	Thermomechanical Treatment	26
4.2.1	Hot Rolling Set Up	30
4.2.2	Thermomechanical Process Schedules	30
4.3	Specimen Design and Preparation	31
4.4	Mechanical Testing	32
4.4.1	Tensile Testing	32
4.4.2	Testing for LCF	32
4.4.3	Testing for HCF	32
4.4.4	Hardness Testing	35
4.4.5	Data Analysis	35
4.5	Metallographic Examination	35
4.5.1	Sample Preparation	35
4.5.2	Optical Metallography	36
4.5.3	Scanning Electron Microscopy	36
4.5.4	Quantitative Metallography	36
	(a) Manual Method	
	(b) Using Image Analyser	
4.6	Fractography	36
5.	Results and Discussion	
5.1	Effect of Thermomechanical Processing of 38MnSiVS5 on its Microstructural Evolution	37
5.1.1	Effect on Inter-Lamellar Spacing of Pearlite	44
5.1.2	Effect on Ferrite-Pearlite Volume Fractions	45
5.1.3	Effect on Grain Size of Ferrite	45
5.2	Effect of Thermomechanical Processing of 38MnSiVS5 on Tensile Properties	47
5.3	Effect of Thermomechanical Processing of 38MnSiVS5 on Hardness	50
5.4	Effect of Thermomechanical Processing of 38MnSiVS5 on LCF Behavior	51
5.4.1	Cyclic Stress Response	51

5.4.1.1	TMP1 (Polygonal Ferrite/Fine Pearlite)	51
5.4.1.2	TMP2 (Polygonal Ferrite/Medium Pearlite)	51
5.4.1.3	TMP3 (Polygonal Ferrite/Coarse Pearlite)	51
5.4.1.4	TMP4-TMP6	53
5.4.2	Cyclic Stress – Strain Curve	58
5.4.3	Coffin-Manson and Basquin Plots	60
5.4.4	Fatigue Life Assessment	69
5.5	Effect of Thermomechanical Processing of 38MnSiVS5 on HCF Behavior	70
5.6	Fractography	73
6.	Conclusions and Suggestions for Future Work	
6.1	Conclusions	80
6.2	Suggestions for Future Work	81

References

List of figures

	Page No.
Figure 4.1 Optical Micrograph of as received material : (a) In the cross direction (b)Same as (a) at higher magnification	27
Figure 4.2 Optical Micrograph of as received material : (a) In the longitudinal direction (b)Same as (a) at higher magnification.	28
Figure 4.3 SEM Micrograph of as received material : (a) In the cross direction (b)In longitudinal direction	29
Figure 4.4 The dimensions of the fatigue test samples used in the present investigation.	33
Figure 4.5 A typical hysteresis loop obtained in a strain controlled test used to measure the total and plastic strain amplitudes.	34
Figure 5.1 The optical micrographs of 3TMP conditions in cross(normal to rolling)direction : (a) TMP1(PF/FP) (b) TMP2(PF/MP) (c) TMP3 (PF/CP).	38
Figure 5.2 The optical micrographs of 3TMP conditions in longitudinal(in the plane of rolling)direction : (a) TMP1(PF/FP) (b) TMP2(PF/MP) (c) TMP3 (PF/CP).	39
Figure 5.3 The SEM micrographs of 3TMP conditions in cross(normal to rolling)direction : (a) TMP1(PF/FP) (b) TMP2(PF/MP) (c) TMP3 (PF/CP).	40
Figure 5.4 The SEM micrographs of 3TMP conditions in longitudinal(in the plane of rolling)direction : (a) TMP1(PF/FP) (b) TMP2(PF/MP) (c) TMP3 (PF/CP).	41
Figure 5.5 The optical and SEM micrographs of TMP6 Condition (a) Optical (b) SEM.	42

Figure 5.6	(a) Continuous cooling transformation (CCT) diagram after austenitization at 1200°C. (b) Interaction of recrystallization R and precipitation P.	46
Figure 5.7	Monotonic engineering stress – strain curve for the three different TMP conditions as well as-received material.	49
Figure 5.8	Cyclic stress response of the TMP1(PF/FP) condition at different total strain amplitude.	54
Figure 5.9	Cyclic stress response of the TMP2(PF/MP) condition at different total strain amplitude.	54
Figure 5.10	Cyclic stress response of the TMP3(PF/CP) condition at different total strain amplitude.	55
Figure 5.11	Cyclic stress response of the TMP4 condition at different total strain amplitude.	56
Figure 5.12	Cyclic stress response of the TMP5 condition at different total strain amplitude.	57
Figure 5.13	Cyclic stress response of the TMP6 condition at different total strain amplitude.	57
Figure 5.14	Cyclic stress-strain curves for the three microstructural conditions as obtained by constant total strain amplitude controlled tests. Stabilized or half-life stress values were obtained from the stress response curves.	59
Figure 5.15	Coffin-Manson Plots for the three conditions	61
Figure 5.16	Total strain amplitude as a function of reversals to failure for the three TMP conditions.	62
Figure 5.17	Cyclic total ,elastic and plastic strain amplitudes plotted as a function of number of load reversals to failure, $2N_f$. the intersection of elastic and plastic strain is the transition life $(2N_f)_t$	63
Figure 5.18	Life predicted by MUS model (a) TMP1 (PF/FP) (b) TMP2 (PF/MF) (c) TMP3 (PF/CF)	64-65
Figure 5.19	Life predicted by Tomkins' Model (a) TMP1 (PF/FP) (b) TMP2 (PF/MF) (c) TMP3 (PF/CF)	66-67

Figure 5.20	High Cycle Fatigue behavior of the TMP1&TMP2 conditions. The endurance limit is indicated by arrows.	71
Figure 5.21	The elastic strain amplitude Vs No. of reversals to failure ($2N_f$) , TMP1 & TMP2 conditions.	72
Figure 5.22	(a) Crack initiation at an intrusion on the surface in PF/CP material (b) Stage I fatigue propagation in PF/CP material.	75
Figure 5.23	(a) Crack propagation by micro void coalescence in PF/CP material. (b) Enlarged view of (a)	76
Figure 5.24	Striations associated with crack growth in PF/CP material.	77
Figure 5.25	(a) Fatigue striations in PF/FP material. (b) Micro void growth and coalescence in PF/FP material.	78
Figure 5.26	Shearing of Inclusion.	79

List of Tables

		Page No.
Table 1.1	Design philosophies against fatigue failure	3
Table 2.1	General Comparison of mild steel with various high strength steels [Metals Handbook, 1990]	6
Table2.2	Effect of selected elements on the properties of microalloyed steels [Wright, 1990]	17
Table 4.1	Chemical composition of 38MnSiVS5	26
Table 4.2	Details of thermomechanical process Schedules	31
Table 5.1	Microstructural Properties of 38MnSiVS5 in normal to rolling direction (i.e. in Cross direction).	43
Table 5.2	Microstructural Properties of 38MnSiVS5 in the plane of rolling (i.e. in Longitudinal direction)	44
Table 5.3	Room temperature tensile properties of 38MnSiVS549	50
Table 5.4	Hardness of Three microstructures and as received material.	50
Table 5.5	Parameter describing the CSS curves for three microstructural conditions	58
Table 5.6	Room temperature cyclic properties of material having three different microstructures	69
Table 5.7	High cycle fatigue properties of 38MnSiVS5	73

Chapter 1

Introduction

The word fatigue originated from the Latin expression *fatigare*, which means ‘to tire’. Although commonly associated with physical and mental weariness in people, the word fatigue has also become a widely accepted terminology in engineering vocabulary for the damage and failure of materials under cyclic loads [Suresh, 1997]. ‘Fatigue’ of materials, structures and components was first reported in the 1800s when several investigators in the Europe observed that bridges and railroad components were cracking when subjected to repeated loading. As the century progressed and the use of metals expanded with increasing use of machines, more and more failures of components subjected to repeated loads were recorded. The dramatic effect of subcritical crack growth by fatigue on the mechanical integrity of the aircraft structures was clearly brought to light by the series of crashes involving first commercial jet airliner, the Comet [Suresh, 1997]. Even though much progress has been made, developing design procedures to prevent failure from fatigue is still a daunting task. It involves the interplay of various field of knowledge, namely, materials engineering, manufacturing engineering, structural analysis (including loads, stress, strain and fracture mechanics analysis), non-destructive inspection and evaluation, reliability engineering, testing technology, field repair and maintenance, and holistic design procedures. All these must be placed in a consistent design activity that may be referred to as fatigue design policy. With increased understanding of materials, which accelerated in the early 1900s, a considerable amount of knowledge is available on repeated load effects on engineering materials. The procedures that have been evolved to deal with repeated loads in design can be reduced to three.

- The stress life approach
- The strain life approach
- The damage tolerance approach

1.1 Definition

ASTM 1150, annual book of standards, defines the term fatigue as “fatigue(Note1): the process of progressive localized structural change occurring in a material subjected to conditions that produce fluctuating stresses and strains at some point or points and that may culminate in cracks or complete fracture after a significant number of fluctuations(Note2). Note1-In glass technology, static tests of considerable duration are termed ‘static fatigue’ tests, a type of test generally designated as stress-rupture. Note2-Fluctuations may occur both in loads and with time(frequency) as in the case of ‘random vibrations’ ”.

1.2 Industrial Significance

There is little doubt that fatigue plays a significant role in all industrial design applications. Many components are subjected to potentially detrimental loads. However, it is imperative that all designs consider those aspects of nucleation process other than fatigue that could propagate under the influence of cyclic loads. An important engineering advance is the transfer of multi-stage fatigue process from the field to the laboratory for scientific investigation. In order to study, explain and qualify component design, a key engineering step is often the simulation of the problem in the laboratory. Any simulation is ,of course, a compromise of what is difficult to quantify. But the study of multi-stage fatigue process has been greatly advanced by the combined methods of strain control testing and the development of fracture mechanics of fatigue crack growth rates. This combined approach is a key advance that allows better understanding and simulation of localized strain and the subsequent growth mechanism outside the plastic zone. This integration of fatigue mechanics has had important implications in many industrial applications and materials engineering.

1.3 Design philosophies against fatigue

Design philosophies against fatigue are as shown in Table 1.1 .

Table 1.1 Design philosophies against fatigue failure

Design philosophy	Design methodology	Data description
Safe Life ,infinite life	Stress –life	S-N
Safe life, finite life	Strain –life	$\epsilon - N$
Damage tolerance	Fracture mechanics	$Da/dN - \Delta K$

Safe life design philosophy based on the infinite life criterion reflects the classical approach to the fatigue and is categorized as the high cycle fatigue (HCF) methodology (S-N curve) with most consideration being based on the maintenance of elastic behavior in the sample /component/assembly examined. With advanced and highly loaded components, the stress–life based approach would not be sufficient to handle the full range of the problems to be addressed using continuum assumptions due to the occurrence of the plasticity and the attendant lack of the proportionality between stress and strain. This has led to the use of strain as a controlling parameter. Strain –life is the general approach employed for continuum response in the safe life, finite life regime .It is primarily intended to examine the low cycle fatigue (LCF)domain. Both the above approaches are appropriate for situations where a component or structure can be considered to be a continuum, i.e., those meeting ‘no cracks ‘assumption. When a crack-like discontinuity is present, both the above approaches are not useful. The stress intensity factor, $K=\sigma\sqrt{\pi a}$, (where σ is the stress amplitude and a is the crack length)which is fundamental to LEFM, provides a tractable controlling quantity and material parameter[Cameron, Allegany and Hoeppner,1996].This fracture mechanics parameter, typically the stress intensity range, ΔK ($\Delta K = \Delta\sigma\sqrt{\pi a}$, $\Delta K=K_{\max}-K_{\min}$, K_{\max} =maximum stress intensity factor , K_{\min} = minimum stress intensity factor; $\Delta\sigma=\sigma_{\max}-\sigma_{\min}$,

σ_{\max} =maximum stress amplitude, σ_{\min} =minimum stress intensity amplitude) is related to the crack growth rate under the imposed cyclic loads. Property description for crack extension is typically in terms of crack growth rate (da/dN) vs. stress intensity range (ΔK) plotted on a log-log scale. The use of the stress intensity values and appropriate material properties allows the number of cycles for the crack growth over a range of crack sizes to be estimated and fracture to be predicted.

Literature Review

INTRODUCTION

2.1.1 The rationale of Microalloyed High Strength Steels

The motivation for the use of high strength low alloy (HSLA) steel is cost reduction. Higher strength steels can sustain service loads over thinner sections, thus providing weight savings and use of less steel. Lower costs can also be realized if microalloyed steels can replace alloy steels containing significant amounts of expensive elements like Nickel, Chromium or Molybdenum. However, the most significant cost reduction provided by microalloyed HSLA steels is the elimination of expensive heat treatment and their use in the mill processed condition, as-rolled, which provides considerable energy saving. As-rolled microalloyed HSLA steels exhibit properties which are comparable in many ways to those of normalized or quenched and tempered products, yet avoid the cost of heat treatment, handling, energy decarburization, scale loss (oxidation) etc.

In terms of mechanical properties, the heat-treated (quenched and tempered) low alloy steels offer the best combination of strength and toughness (Table 2.1) [Metals Handbook, 1990]. However, these steels are available primarily as bar and plate products and only occasionally as sheet and structural shapes. In particular, structural shapes (I-beams, channels, wide flanged beams, or special sections) can be difficult to produce in the quenched and tempered condition because shape warpage can occur during quenching. Heat treating steel is also a more involved process than the production of as-rolled steels, which is one reason why as-rolled steels are an attractive alternative. The as-rolled HSLA steels are also commonly available in all the standard wrought forms (sheet, strip, bar, plate and structural shapes).

Table 2.1 General comparison of mild steel with various high strength steels [Metals Handbook, 1990]Chemical Composition (%)^a

Steel	C (max.)	Mn (max.)	Si (min)	Other	Min. Yield Strength (Mpa)	Min. UTS (Mpa)	Min.Ductility ^b (%) ^c
Low-Carbon steel	0.29	0.60	0.15	(c)	170-250	310-445	23-30
As-hot rolled C-Mn steel	0.40	1.00	0.15	250-400	415-690	15-30
HSLA steel	0.08	1.30	0.15	0.02 Nb	275-450	415-550	18-24
Heat treated C steel Normalized ^c	0.36	0.90	0.15		200	415	24
Quenched and Tempered	0.20	1.50	0.15	5 ppm B	550-690	660-760	18
Q and T low-alloy steel	0.21	0.45	0.20	0.45 Mo, 50 ppm B	620-690	720-800	17-18

^aTypical compositions include 0.04% P (max.) and 0.05% S (max.)^bElongation in 50 mm gage^cIf copper is specified, the minimum is 0.20%

In general the rationale behind the development of these steels can be summarized as:

- Filling the yield strength gap between the simple carbon and mild steels with $\sigma_y \sim 300$ MPa and heat-treated low alloy steels with $\sigma_y \sim 850$ MPa with a mill processed microalloyed steel not requiring a separate heat treatment operation.
- Producing high yield strength so that a greater load bearing capacity is possible with thinner sections.
- Decreased processing costs, and obtaining a higher yield strength material, by using mill-processed steel with consequent energy conservation.
- A minimal use of expensive and scarce alloying addition, with the consequent conservation of strategic scarce materials.
- High weldability.
- A high resistance to brittle cleavage and low energy ductile fracture, and a low ductile-brittle transition temperature.
- An ability to cold form to some extent, particularly by bending and good ductility and toughness through the thickness of rolled strips and plates.
- Optimal property combinations per unit cost.

These requirements have been met by three main classes of material microstructures:

Steels comprising ferrite -pearlite microstructures, which will be the main subject of this discussion. Acicular ferrite structures, which may be considered to be very low carbon variants of bainitic steels developed in the early 1950' s. These are less popular than the ferrite-pearlite structures, largely due to increased cost. Dual phases microstructures, which were developed specifically to increase the formability and aimed particularly for use in the manufacture of automobile components.

2.1.2 Applications of HSLA Steels

HSLA steels were first used as structural shapes and plates in the early 1960' s because of their ability to be welded with ease. By the early 1970' s, they were also used in pipelines at both elevated temperature and severe arctic conditions. Later in the 1970's, concurrent with the energy crisis, another dominant application involved the use of HSLA steels to reduce the weight of parts and assemblies in trucks and automobiles. In the 1980's, bars, forgings and castings have emerged as applications of particular interest. Shapes such as elbows and fittings for pipelines are also being cast out of microalloyed steel. HSLA steels are used in a wide variety of applications, and their properties can be tailored to specific applications by a suitable combination of composition and microstructures obtained by processing in a mill. For example, low -carbon and closely controlled carbon equivalent values provide good toughness and weldability. Good yield strength and fracture toughness results from a fine grain size.

Oil and gas pipelines. While tensile strength is a key requirement in pipelines, other properties are no less critical for the fabrication and operation of oil and gas pipelines. They include weldability, fracture toughness and corrosion resistance, which are met by HSAL steels.

Automotive applications. Experience in the application of cold- and hot-rolled HSLA sheet in automotive applications indicates the importance of requirements with respect to stiffness, crash behavior, fatigue life, corrosion resistance, acoustic properties and of course, formability and weldability. In addition to improvement in mileage per unit fuel consumption through weight reduction, benefits may be found in increasing payloads without a change in fuel consumption. Candidate applications here include trucks, rail cars, off-highway vehicles and ships. Ship applications are however limited by buckling and stiffness considerations.

Offshore applications. The essential characteristics of steels for these applications include:

- Yield strength in the regions of 350 to 415 MPa.

- Good weldability.
- High resistance to lamellar tearing.
- Lean compositions to minimize preheat requirements.
- High toughness in the weld heat-affected zone.
- Good fracture toughness at the designated operating temperatures.

Some of these goals have been realized through a reduction in impurities such as sulphur, nitrogen and phosphorus in the steelmaking process. Controlled rolling and accelerated cooling of niobium steels have allowed a reduction in carbon contents, which is important to enhance weldability. Modification of sulfide inclusions is done by additions of rare-earth elements or calcium to form spheroidal inclusions. This approach usually results in both the elimination of lamellar tearing and an improvement in transverse impact properties. Bars, forgings and castings have emerged as the latest area of opportunity for microalloyed HSLA steels, and there has been a rapid assimilation of technologies developed in other product areas. In particular, the search is on for higher strengths, elimination or reduction of heat treatments, simplified cold finishing or machining operations, and improved toughness, machinability and weldability.

2.2 Growth of Microalloyed Steels

Starting with plain carbon steels containing 0.3 wt. % C, little importance was attached to yield strength, toughness or weldability of HSLA steels, design being based on tensile strength. This was standard steel in the late 1930's.

2.2.1 Grain Refined Steels

By the early 1950' s the beneficial effect of ferrite grain refinement on yield strength and the ductile-brittle transition temperature had been demonstrated (Petch, 1953; Cracknell and Petch, 1955]. Initially, grain refining used Al-N additions (Weister and Ulmer, 1959]. Later other grain refining additives like niobium, titanium or vanadium

also were found to contribute to precipitation strengthening and higher yield strengths (Thomson and Krauss, 1989; Irvine et al. 1970).

2.2.2 Precipitation Strengthening

It was found that grain refinement could take place in niobium steels, but no precipitation strengthening was present if the normalizing or austenizing temperature was a conventional $A_{c3} + 30$ °C. With higher normalizing temperatures, precipitation strengthening became progressively greater but only at the expense of a pronounced loss in toughness. On the other hand, vanadium steels showed precipitation strengthening when normalized from conventional temperatures and the impact toughness was greater than in the niobium steels [Honeycombe, 1986].

2.2.3 Development of Controlled Rolling

The use of controlled rolling at a low finish rolling temperature is to produce fine recrystallized or elongated unrecrystallized austenite grain morphologies, which then transforms to fine polygonal ferrite on cooling to give excellent yield strength and associated toughness [Irvine et al., 1970; Phillips and Chapman, 1966; Duckworth, 1965]. Much detailed research to understand the mechanisms present during controlled rolling has been carried out [Tanaka, 1981; Tamura et al., 1988]. Conventional controlled rolling was able to increase the yield strength to 450-525 MPa with the impact transition temperature (ITT) as low as -80 °C.

2.2.4 Development of Controlled Cooling

The development of controlled cooling, J.e., accelerated cooling of either a plate, or more particularly of hot rolled strips, followed quickly the development of controlled rolling. The reason for this was that the ferrite grain size decreases with decreasing austenite to ferrite transformation temperature with a consequent improvement in both yield strength and toughness (lower impact transition temperature, ITT). Accelerated cooling of plate materials can be carried out by air circulation, water sprays or mist cooling, but care is necessary to prevent excessive surface cooling and the formation of martensite/bainite structure. Lamellar flow cooling is widely used for accelerated cooling of hot strip mill products [Sigalla, 1957].

2.2.5 Low carbon ferrite-pearlite Steels

In the 1960's the use of exceptionally low carbon pearlite free steels was considered. The economic and production difficulties with these steels led to somewhat higher carbon contents of 0.03 to 0.08 wt.%, the pearlite reduced steels. These steels produced yield strengths of 550 MPa and an ITT of- 70°C [Phillips and Chapman, 1966].

2.2.6 Acicular Ferrite Steels

In the 1950's, low carbon (0.12/0.15 wt%) bainitic steels were developed on a commercial scale. The proof stress values of 450-900 MPa, depending on the carbon content and transformation temperature, had an advantage over the ferrite-pearlite HSLA steels, but the toughness was considerably inferior so that interest in bainitic steels waned a ferrite-pearlite steels of lower alloy content and good strength - toughness combinations were developed. The work of Coldren et al. (1978) led to commercially attractive alloys based on 0.03 wt.% C, manganese-molybdenum-niobium that were produced as hot rolled strips for line pipes. This steels was produced with fully acicular ferrite bainite structures, with a modest yield strength of about 500 MPa and a very low ITT.

2.2.7 Dual phase steel

HSLA steels showed low stretch formability. The problem was resolved by processing a conventional HSLA steel, usually one containing vanadium and often with an enhanced nitrogen content of 0.015 wt.% [Davies, 1978; Owen, 1980], in such a way as to change the microstructure from one of ferrite-pearlite to one of ferrite containing islands of martensite-austenite to introduce continuous yielding and a high work hardening rate. However, there are problems concerning spring back and control of the processing treatment.

2.2.8 Inclusion Shape Control

The elongation of non-metallic inclusion, which occurs during rolling of steel, is responsible for the anisotropy in ductility and toughness. The effects of elongated co-

planar arrays of manganese sulfide are generally considered most deleterious, because they lead to lower ductility and toughness values in the transverse direction. Around 1965 it was realized that these elongated or co-planar arrays are detrimental to longitudinal bending of hot rolled strips [Korchynsky and Stuart, 1970] and caused lamellar tearing in highly restrained welds in thick plates [Farrar, 1971]. The problem has, however, been overcome by the important development of inclusion shape control technology in which the plasticity of MnS inclusions is decreased by the addition of zirconium [Michelich et al., 1971], cerium [Little and Henderson, 1971], or calcium [Hilty and Popp, 1969], so that elongated stringers are not produced.

2.3 Classifications

HSLA steels can be divided into the following six categories:

- Weathering steels, which contain small amounts of copper and phosphorus, and display improved atmospheric corrosion resistance and solid solution strengthening.
- Microalloyed ferrite-pearlite steels, which contain very small additions of strong carbide or carbonitride forming elements such as niobium, vanadium and/or titanium for precipitation strengthening, grain refinement and transformation control.
- As-rolled pearlitic steels, which may include carbon-manganese steel but which also have small addition of other alloying addition to enhance strength, toughness, formability and weldability.
- Acicular ferrite steels, which are low carbon steels with an excellent combination of high yield strength, formability, weldability and toughness.
- Dual-phase steels, which have a microstructure of martensite dispersed in a ferrite matrix and provide a good combination of ductility and high tensile strength.
- Inclusion shape controlled steels; which provide improved ductility and toughness by small addition of calcium, zirconium or titanium, or rare- earth elements so that

the shape of sulfide inclusion are changed from elongated stringers to small, dispersed, almost spherical globules.

2.3.1 Microalloyed Ferrite-Pearlite Steels

The yield strength , σ_y , is given in general terms by:

$$\sigma_y = \sigma_i + \sigma_s + \sigma_p + \sigma_d + k_y d^{-1/2}$$

where σ_i is the friction stress opposing dislocation motion, σ_s is the contribution from solid solution strengthening, σ_p is due to precipitation strengthening, σ_d is because of dislocation strengthening, k_y is the dislocation locking term and d is the ferrite grain diameter. Using well known theories of strengthening and work hardening of structures comprising unreformed particles in an unreformed matrix [Ashby,1966; Brown and Stobbs, 1971] it has been shown that the flow stress and the work hardening rate can be predicted accurately [Ballinger and Gladman, 1981; Lanzillotto and Pickering, 1982]. The flow stress and the work hardening rate are controlled by the volume fraction and the particle size of the M-A constituent. Theories predict that both the flow stress and the work hardening rate should be related linearly to the reciprocal of the square root of the size of the M-A particles.

These steels use additions of niobium and vanadium to increase the strength of hot rolled steel without an increase in the carbon and/or manganese contents. various types of microalloyed ferrite-pearlite steels include:

- Vanadium-microalloyed steels
- Niobium-microalloyed steels
- Niobium-molybdenum steels
- Vanadium-niobium microalloyed steels
- Vanadium-nitrogen microalloyed steels
- Titanium-microalloyed steels

- Niobium-titanium microalloyed steels
- Vanadium-titanium microalloyed steels

Vanadium containing steels are used in the hot-rolled condition and also in the controlled-rolled, normalized, or quenched and tempered condition. Strengthening from vanadium averages between 5 and 15 MPa per 0.01 wt. % V [porter, 1986] depending on carbon content and cooling rate. An optimal level of precipitation strengthening occurs at a cooling rate of about $17^{\circ}\text{C min}^{-1}$. Manganese content and ferrite grain size also affect the strengthening of vanadium microalloyed steels [Meyer et al., 1977]. The effect of manganese on precipitation strengthening is more in vanadium steels than in niobium steels.

2.4 Role of Microalloying Elements

Alloying elements are selected to influence the transformation temperatures so that the transformation of austenite to ferrite and pearlite occurs at a lower temperature - during air-cooling. This lowering of the transformation temperature produces a finer grain transformation product, which is the main source of strengthening. At the low carbon levels typical of HSLA steels, elements such as silicon, copper, nickel and phosphorous are particularly effective for producing fine pearlite. The microalloying elements Nb, V and Ti are added singly or in combination to what are essentially carbon-manganese steels, to produce the HSLA steels. These three microalloying elements have very different effects due to their different affinities for carbon and nitrogen. Microalloying elements are added to steel for two main purposes, namely, to grain refine and/or precipitation strengthening. Both effects result from the precipitation of microalloy carbides, nitrides or carbonitrides. These precipitates in ferrite can prevent ferrite grain growth during or after the transformation and so have an indirect grain refining effect. It must be emphasized, however, that microalloy carbides/nitrides precipitated in the austenite do not cause strengthening.

2.4.1 Solubility Effects

The solubility of the microalloy carbides/nitrides in austenite decreases in the

following order: TiN, NbN, TiC, VN, NbC, VC and the same order is followed for the solubility in ferrite in which the solubility is some two orders of magnitude smaller than in austenite. A general solubility product equation is:

$$\log[M][X]=A/T+B$$

where [M] and [X] are the weight percent of microalloying element and C or N dissolved in the austenite at T Kelvin, and A and B are constants.

2.4.2 Grain Refinement

The essence of grain refinement is to prevent grain boundary migration and grain growth. This may be done either by grain boundary solute segregation introducing a frictional drag on the moving boundary or by grain boundary pinning particles which decrease the grain boundary area and hence the overall grain boundary energy.

If the grain size is to remain small at the high temperature in the austenite region, such as what is used for reheating for hot rolling, and especially for re crystallization controlled rolling (RCR), two conditions are to be satisfied (Gladman and Pickering, 1967]:

- (i) the volume fraction of pinning particles must remain large, and
- (ii) the pinning particles must grow only very slowly at the temperature involved.

The low solubility and general thermodynamic stability causes TiN to be the most resistant of the microalloying carbides/nitrides to particle coarsening, and thus the most effective grain boundary pinning phase. This partially explains why Ti microalloying is used in recrystallization controlled rolled steels.

2.4.3 Precipitation Strengthening

In Nb steels the strengthening precipitates are predominantly NbC and in Ti steels TiC. Due to the restricted solubility of Ti in the austenite, strengthening by TiC requires rather high Ti additions compared to the 0.01/0.02 wt. % required for optimal grain refinement. A higher austenizing temperature will also be required. Thus, Ti additions are not predominantly used for precipitation strengthening in many steels. In contrast, due to the much increased solubility of VC, V additions are mainly made for precipitation strengthening and unlike NbC, the solubility and hence the precipitation potential is not greatly limited by the carbon content, either due to additional VN precipitation or N being dissolved in VC as V(CN). Also, decreasing the transformation temperature produces finer precipitates, and greater strengthening.

2.4.4 Alloying Elements

Vanadium: Precipitation strengthening is one of the primary contributors to strength in microalloyed steels; it is most readily achieved with vanadium additions in the 0.03 to 0.10 wt.% range. Vanadium also increases toughness by stabilizing dissolved nitrogen. The impact transition temperature also increases when vanadium is added.

Niobium: Niobium can also have a strong precipitation strengthening effect provided it is taken into solution during reheat and is kept in solution during forging. Its main contributions, however, are to form precipitates above the transformation temperature and to retard the recrystallization of austenite, thus promoting a fine-grained microstructure having improved strength and toughness. Concentrations vary from 0.020 to 0.10 wt.% Nb.

Titanium: Titanium can behave both as a grain refiner and precipitation strengthener, depending on its content. At compositions greater than 0.050 wt. %, titanium carbides begin to exert a strengthening effect. However, at this time, titanium is used commercially to retard austenite grain growth and thus improve toughness. Typically titanium concentrations range from 0.01 to 0.020 wt.%.

Molybdenum: Molybdenum in hot rolled HSLA steels is used primarily to improve hardenability when transformation products other than ferrite or pearlite is desired. It also greatly simplifies the process controls necessary in the forge shop.

Manganese: Manganese is generally present in larger quantity in HSLA steels than in structural carbon steels. It functions mainly as a mild solid solution strengthener in ferrite and also provides a lowering of the austenite to ferrite transformation temperature. In addition, it improves the notch toughness of HSLA steels. In steels for welding application, Mn should be kept below some maximum value that depends on the overall composition but mainly on the carbon content.

Silicon: Silicon is usually present in fully deoxidized steels in amounts up to 0.35%. Silicon has a strengthening effect in low alloy structural steels. In larger amounts it reduces scaling at elevated temperature. Silicon has a significant effect on yield strength enhancement by solid solution strengthening. Effects of selected elements on the various factors discussed above are given in Table 2.2.

Table 2.2 Effect of selected elements on the properties of microalloyed steels [Wright, 1990]

Elements	Precipitation Strengthening	Ferrite grain refinement	Nitrogen fixing	Structure modification
Vanadium	Strong	Weak	Strong	Moderate
Niobium	Moderate	Strong	Weak	None
Molybdenum	Weak	None	None	Strong
Titanium	Strong(<0.05%Ti)	Strong	Strong	None

2.5 Steel-Making

In general, from the point of view of steel making HSLA steels are not difficult to produce. Niobium does not have a strong affinity for either nitrogen or oxygen in

liquid steel, and therefore can be added to steels which show a wide range of levels of deoxidation and solidification rates,

Vanadium, like niobium, has no strong deoxidizing effect in liquid steel but, due to greater solubility of its carbides/nitrides compared with those of Nb, it is less susceptible to strain induced precipitation and therefore produces less severe loss of hot ductility than does Nb.

Titanium has a strong affinity for O, N and S and also for C, and therefore poor and variable recoveries of Ti are experienced unless the steel is quite heavily deoxidized, for example by Al. Inert gas shrouding of liquid metal is required to prevent oxidation of Ti by air.

2.6 Thermomechanical Treatments for Sheets, Strips and Plates

The aim of processing of HSLA steel is to condition the austenite that it transforms to produce the finest ferrite grain size in order to achieve the greatest yield strength consistent with optimal toughness and ductility.

2.6.1 Thermomechanical Working and Controlled Rolling

It is required that in order to produce the finest ferrite grain size, the thermomechanically worked austenite should, during transformation, exhibit a high ferrite nucleation rate and a low ferrite growth rate. In addition, the nucleation and growth of microalloy carbides/nitrides are of utmost importance.

The requirements to produce the necessary fine ferrite grain size are greatest area of austenite grain boundary for ferrite nucleation. Such nucleation can occur on deformation bands in the unrecrystallized austenite, on the recovered sub-structure boundaries, particularly if these contain precipitates, and on undissolved carbide/nitride particles [Amin and Pickering, 1982].

In order to obtain the finest possible ferrite grain size, not only the initial austenite grain size should be as fine as possible but also the temperature of rolling should be as low as possible provided it is above the recrystallization stop temperature, and the rolling strain should be as large as possible.

Current steels tend to employ combinations, e.g. Nb- V. The NbC or VN (using enhanced nitrogen) tend to restrict grain growth, whilst the more soluble VC is used to precipitation strengthen the ferrite. Microalloying additions also have another important effect during controlled rolling, in that they retard recrystallization. The effect seems to be in the ascending order of effectiveness: Mn, Al, V, Nb and Ti on an atomic percentage basis is well established that the recrystallization stop temperature of the austenite increases in the increasing order: V, Al, Ti, Nb. The importance of retardation on recrystallization during controlled rolling lies in the ability to use a low finish rolling temperature to produce elongated unrecrystallized austenite grains, which can transform to very fine polygonal ferrite [Tanaka et al., 1977].

2.6.1.1 Conventional Low Temperature Controlled Rolling

Tanaka (1981) identified the processing parameters to condition the austenite to produce the finest ferrite grain size and optimum precipitation strengthening, using conventional low temperature controlled rolling as:

- (a) a low reheating temperature to produce a fine initial austenite grain size;
- (b) austenite grain refinement by recrystallization;
- (c) suitable pass schedules and reductions to obtain in the initial roughing passes a fine, uniform recrystallized austenite;
- (d) delay between roughing in the recrystallization regime and finishing in the unrecrystallized regime;
- (e) suitable reductions in the unrecrystallized regime below the recrystallization stop temperature, and in some cases finishing below the A_{r3} .

2.6.1.2 Recrystallization Controlled Rolling

Much work has been done in recent years on recrystallization controlled rolling [Roberts, 1984; Roberts et al., 1984; Zheng et al., 1984; Fix et al., 1986; Korchynsky, 1990]. An initial very fine austenite grain size is required prior to rolling and this is

achieved by addition of Ti to form TiN. Such particles very effectively pin the austenite grain boundaries and inhibit grain growth. Rolling is then carried out above the recrystallization stop temperature so that repeated recrystallization occurs during deformation sequences. The finest recrystallized austenite grain sizes are produced by heavy rolling reductions at the lowest possible temperature above the recrystallization stop temperature. The fine recrystallization austenite grains have a high grain boundary surface area per unit volume, i.e. a high S_v , and thus provide many ferrite nucleation sites. Hence, on transforming the austenite, a very fine ferrite grain size is obtained which can be $10\mu\text{m}$ or less and is produced from a recrystallized austenite $20\mu\text{m}$ or less [Zajac et al., 1990; Korchynsky, 1990]. Using a 0.09 wt. % C, 1.4 wt. % Mn, 0.01 wt. % Ti, 0.08 wt. % V, 0.013 wt. % N steel, recrystallization controlled rolled and cooled at 9°C s^{-1} , one can obtain a yield stress of 450/500 MPa with as ITT of -70°C [Zajac et al., 1990] which is comparable with the properties produced by conventional low temperature controlled rolling.

2.6.2 Controlled Cooling

The purpose of controlled or accelerated cooling is to produce the optimal γ to α transformation temperature so that the finest ferrite grain size is achieved, together with optimal strengthening by microalloy carbide/nitride precipitation. A useful method of refining the ferrite grain size for a given austenite grain size is decrease the transformation temperature. This increases the ferrite nucleation rate and the effect may be achieved by alloying or by increasing the cooling rate. The greater the cooling rate or lower the coiling temperature, the finer is the ferrite grain size from given austenite structure.

Using the well-known solubility relationships to assess the volume fraction precipitates, and the observed effects of coiling temperature on both the ferrite grain size and the precipitate size, it is possible by employing a Petch type equation and an Ashby- Orowan precipitation strengthening equation, to calculate the yield stress as a function of coiling temperature. This can be converted into a nomogram for process control.

2.7 HSLA Forgings

Heat treated forgings currently outperform alternative materials where strength, toughness and reliability are primary considerations. However, methods must be found that achieve these benefits at lower cost.

Unfortunately, the thermomechanical processing used for HSLA flat rolled products cannot be readily transformed to hot forgings. Typical forgings are produced from bars that are induction-heated or gas heated to 1250°C, then hot worked to 1100°C. Grain growth and precipitate coarsening are rapid at these temperatures. Attempts to forge at a lower temperature to optimize the as-forged steel properties result in increased die wear and decreased equipment efficiency.

2.7.1 Metallurgical Effects

Upon cooling from forging temperature, niobium carbide begins to precipitate at about 1205°C. The precipitate continues to form and coarsen as temperature falls to 925°C the absence of hot working Continued hot working-into the 900°C temperature range however, retards austenite recrystallization and precipitation resulting in the development of a refined austenite grain size.

Vanadium carbonitride precipitation begins at about 950°C. Precipitate coarsening during accelerated cooling from the forge temperature is minimal; a maximum precipitation strengthening effect is achieved. Toughness improves when ferrite grain size is minimized by controlling the finish hot-working temperature. The 20J-transition temperature for a niobium containing steel is reduced from 30°C to - 80°C by reducing the finish hot-working temperature from 1050 to 900°C. The improvement is independent of reheat temperature [Metals Handbook, 1990].

2.7.2 Development of HSLA Forging Steels

A West German composition 49MnVS3 was successfully used for automotive connecting rods. The steel was typical of the first generation of microalloy steels with a medium carbon content and additional strengthening through vanadium carbonitride

precipitation. The parts were subjected to accelerated air cooling directly from the forging temperature.

2.7.2.1 First Generation Microalloyed Forging Steels

These steels generally have ferrite-pearlite microstructures, tensile strength above 760 MPa and yield strength in excess of 450 MPa. The room temperature Charpy V-notch toughness of first generation forgings is typically 7-14 J. It became apparent the toughness would have to be significantly improved to realize the full potential microalloy steel forgings.

2.7.2.2 Second Generation Microalloyed Forging Steels

Second generation microalloyed forging steels were introduced in about 1986. These are typified by the West German grade 26MnSiVS7. The carbon content of these steels was reduced to between 0.1 to 0.3%. They are produced with either a ferrite-pearlite microstructure or in acicular ferrite structure. The latter results from the suppression of the pearlite transformation caused by the addition of about 0.1% Mo. Titanium addition is also made to these steels to improve impact toughness further.

One of the primary concern of any steel user is the consistency of the finished part properties. Heat treatment has successfully addressed this concern, and a method must be found to ensure consistency of properties in finished parts made from micro alloyed steels. One disadvantage of the ferrite-pearlite microalloyed steel is that the finished strength and hardness are a function of cooling rate. Cooling rate can vary because of process changes or part geometry. The molybdenum treated steel removes the variable of accelerated cooling from the process, an advantage to the hot forger and end user because conveyors are unnecessary.

2.7.2.3 Third Generation Microalloyed Forging Steels

Third generation microalloyed forging steels went into commercial production in the United States in 1989. These steels differ from their predecessors in that they are

directly quenched from the forging temperature to microstructures of lath martensite with uniformly distributed temper carbides.

The newest generation of microalloyed forging steels has five to six times the toughness at -30°C and twice the yield strength of the second-generation materials. No special forging practices are required except for the use of a water cooling system. In a comparison of third generation microalloyed steels with two standard quenched and tempered carbon and alloy steels (1040 and 4140), the properties of the direct quenched microalloyed grade were very similar to those of quenched and tempered 4140. The hardness of all the three materials tested was 40 HRC.

2.8 Mechanical Properties of HSLA Steels

Blarasin and Farsetti (1989) tested five microalloyed steels containing V, Nb and/or Ni in the carbon range of 0.21 to 0.41 wt.% for tensile and impact properties. Yield strength varied from 590 to 840 MPa and UTS from 800 to 940 MPa. Room temperature impact energy was reported to lie in the range of 80 to 140 J cm⁻². AISI 1141 vanadium microalloyed medium carbon steel in the as forged condition has a yield strength (0.2% offset) of 524 MPa and tensile strength of 875 MPa [Yang and Fatemi, 1995]. Low carbon V/Nb microalloyed steels have been reported to have slightly higher compressive yield stress than the tensile value [Kim and Fine, 1982]. Compressive yield strength for the four steels studied was found to lie in the range of 450-610 MPa. HSLA steels also have lower ductile to brittle transition temperature. Typically a Charpy V-notch fracture appearance transition temperature of -40°C is achieved. Conventional controlled rolling can give excellent combination of strength (yield strength 450-525 MPa) and toughness (ITT as low as -80°C). ITT of low carbon ferrite-pearlite microstructure is given by Glandman and Pickering, (1983) as:

$$\text{ITT}(\text{°C}) = -19 + 44 * (\text{wt. \% Si}) + 700 * (\text{wt. \% N}_{\text{free}})^{1/2} + 2.2 (\% \text{ pearlite}) - 11.5 d^{-1/2}$$

Scope of the Present Investigation

3.1 Material for the Present Investigation

A medium carbon microalloyed forging grade steel 38MnSiVS5 steel was chosen for this investigation. The above steel finds application in structural parts in the automotive industry. The microalloyed steel is used for making crankshafts and connecting rods, which are subjected to fluctuating loads. Therefore, this steel was selected as the candidate material for the present experimental study involving the determination of the fatigue and mechanical properties.

3.2 Objective and Scope of the Present Investigation

The following objective were identified for the present investigation.

1. To carry out thermomechanical processing at various temperatures.
2. To characterize and quantify the microstructure obtained by thermomechanical processing at different temperatures.
3. To examine the microstructures to determine the grain size distribution and mean grain size.
4. To examine the grain shapes of various microstructures.
5. To calculate inter-lamellar spacing as a function of thermal/thermomechanical treatment.
6. To investigate the effects of inter-lamellar spacing/microstructure on the LCF and HCF behavior of the material.
7. To determine the tensile properties of the steel after different thermomechanical treatments.

8. To determine the low cycle fatigue behavior and study cyclic softening/hardening behavior after different thermomechanical treatments.
9. To establish the stress-number of cycles to failure curves and the endurance limit.
10. To analyze the fracture surface resulting from the LCF loading with respect to crack initiation, crack propagation and influence of inclusions on the fatigue life .
11. To compare the cyclic yield strength, endurance limit and cyclic response (with respect to cyclic hardening /softening) of thermomechanically processed 38MnSiVS5 steel with those as-forged material. Also compare these with 49 MnVS3 steel.

Experimental Procedure

4.1 As Received Material

The material used in the present investigation was produced at Tata Iron & Steel Company, Jamshedpur, India. The microalloyed medium carbon forging grade steel 38MnSiVS5 was received in the form of rolled blooms of 65 round corner square shapes (RCS).

4.1.1 Chemical Composition

The chemical composition of 38MnSiVS5 is given in Table 4.1.

Table 4.1 Chemical composition of 38MnSiVS5

Material	C	Si	Mn	P	S	V	N	Cr	Fe
38MnSiVS5	0.38	0.68	1.5	0.022	0.06	0.11	0.006	0.18	Balance

4.1.2 Microstructure

The microstructure of as received 38MnSiVS5 steel was basically polygonal ferrite/coarse pearlite. The Optical micrographs of as received material in cross and longitudinal direction is shown in fig. 4.1. and fig. 4.2 respectively. SEM micrograph is shown in fig. 4.3.

4.2 Thermomechanical Treatment

Thermomechanical Processing in the present investigation was done by hot rolling of the steel by imparting the known amount of area reduction (about 55%) at a given

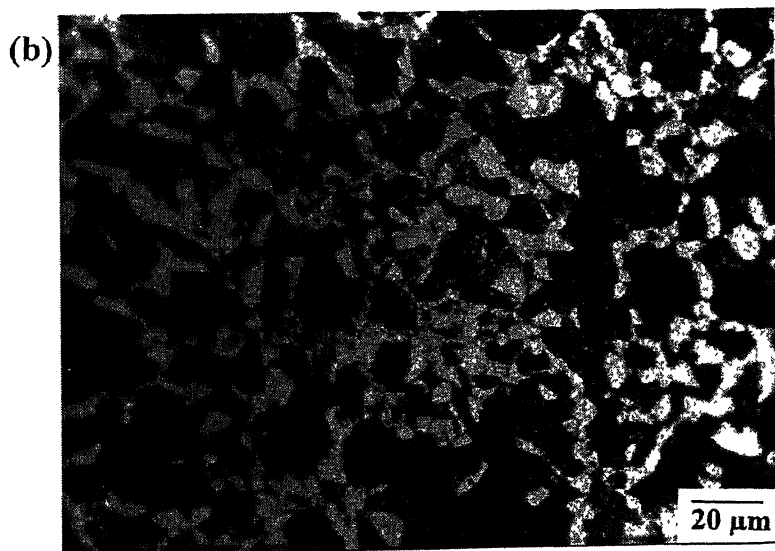
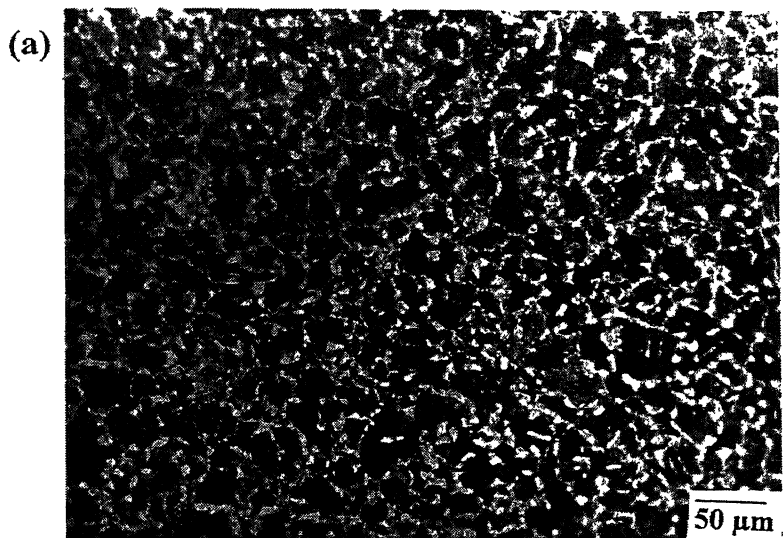


Figure 4.1 Optical Micrograph of as received material (a) In the cross(normal to rolling) direction (b)Same as (a) at higher magnification.

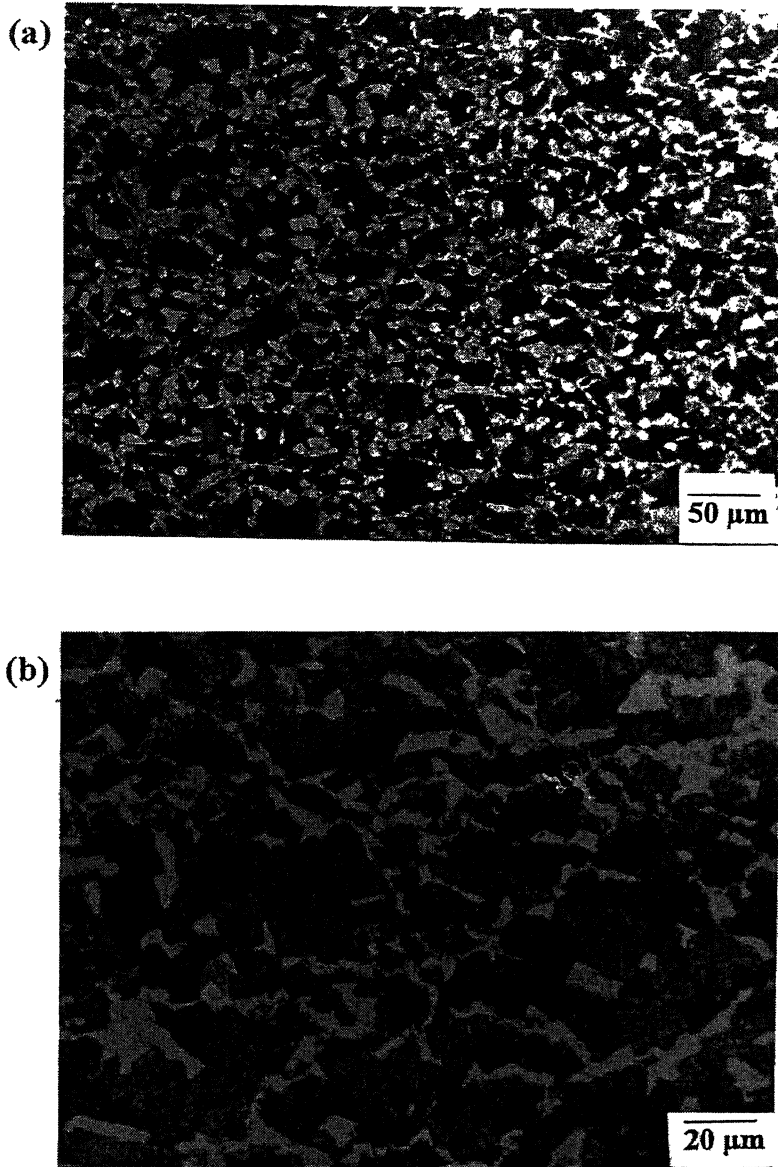
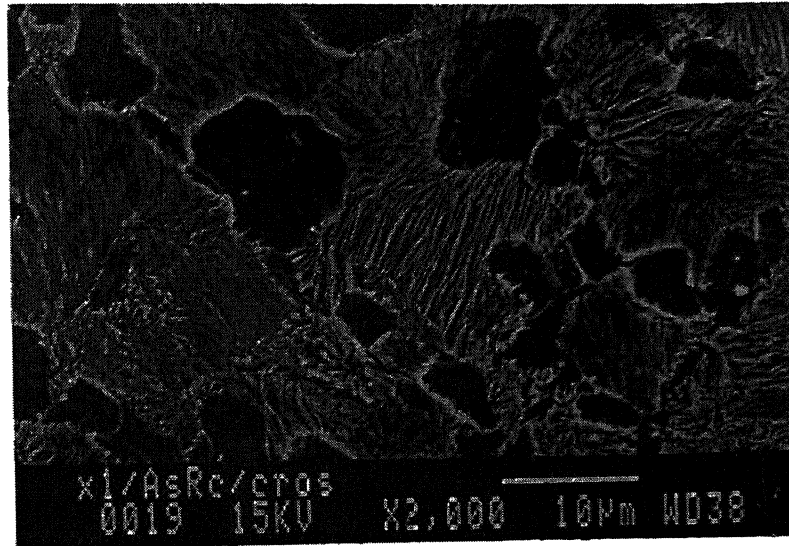


Figure 4.2 Optical Micrograph of as received material (a) In longitudinal (in the plane of rolling) direction (b) Same as (a) at higher magnification.

(a)



(b)

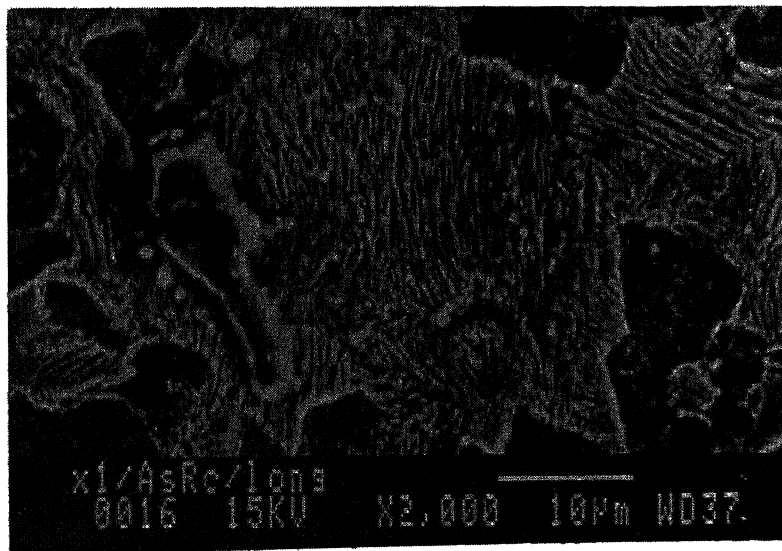


Figure 4.3 SEM Micrograph of as received material (a) In the cross(normal to rolling) direction (b) In longitudinal(in the plane of rolling) direction

temperature either in Austenite or Austenite + Ferrite phase field followed by air cooling. Total 6 schedules of rolling were given. For first 3 schedules of rolling (named as TMP1-TMP3), the samples were directly machined from 65 RCS blooms by cutting into 4 pieces across the cross section and then machining to one inch diameter. For last 3 schedules (TMP4-TMP6), the 65 RCS blooms were reheated to 1150-1250°C, finish forged at around 900°C to one inch diameter individually cooled to 600°C following which they were cooled in a pile. This was the starting material for thermomechanical processing as described in 4.2.2.

4.2.1 Hot Rolling Set Up

Heating and Soaking of the samples was done in a specially designed high temperature furnace, kept very close to the rolling mill. Muffle of the furnace consisted of an inconel tube & was closed from one end. The furnace was heated by silicon carbide rods and had a constant temperature zone of about 17.5 cm long. The heating and soaking of the samples were done in atmospheric air.

Hot rolling of the round specimen of 38MnSiVS5 steel was done on a 2-high rolling mill (FENN model No. 051 Two –High with combination gear – reducer pinion) having rolls of 135 mm diameter. The grooved rolls were used for rolling the samples, which were of the round rod shape. Speed of the rotation for the rolling was kept constant at 72 rpm in all the experiments. No prior heating of the rolls was done before hot rolling of the specimens & they were maintained at room temperature.

4.2.2 Thermomechanical Process Schedules

Hot rolling was essentially multipass in nature. For the first three schedules (TMP1-TMP3), the temperature of the furnace was maintained at 1200° C. The multipass rolling was done in such a way to give area reduction of 55-60% (25.4 mm sample was reduced to 17 mm after rolling in 6-8 passes) till the finish rolling temperature was 800°C, 900°C, 1000°C in TMP1, TMP2, TMP3 respectively. For schedule no 4

to 6, the temp. of the furnace was maintained at 100°C more than the rolling temperature i.e. at 900°C ,1000°C and 1100°C for TMP4 to TMP6 respectively. For these schedules to nullify the temperature drop effect a soaking treatment of 5-10 minutes was given after every 3 passes. All the samples were reduced to about 17mm diameter from 25.4 mm after rolling. The details of thermomechanical processes are given in Table 4.2.

Table 4.2 Details of thermomechanical process Schedules

Process I D No.	Soaking Temp	Inter Pass Reheating Temp	No. of Passes	Finish Rolling Temp	Process Details
TMP-1	1200°C	N/A	6	750-800°C	Soaked at 1200°C for 1 hour. Reduced from 25.4 to 17 mm in 6 passes . No interpass reheating was carried out.
TMP-2	1200°C	N/A	6	870-920°C	- do -
TMP-3	1200°C	N/A	6	970-1020°C	- do -
TMP-4	900°C	900°C	8	750-800°C	Soaked at soaking temp. for 1 hr. Reduced from 25.4 to 17 mm diameter in 8 passes. Reheating carried out after every 3 passes to nullify effect of cooling during rolling.
TMP-5	1000°C	1000°C	8	870-920°C	-do -
TMP-6	1100°C	1100°C	8	970-1020°C	- do -

4.3 Specimen Design and Preparation

Tensile specimens were prepared according to ASTM standard E-8M. Specimens for LCF were prepared according to ASTM standard E 606-80 and those for HCF according to ASTM standard E-466. Due to thickness limitations of the sample after rolling, the width of grip section was kept 1.5 d (1.5 times gage diameter) as against

2d specified by the standards. The grips of the machines were hydraulic & there was no extension on the grip section during the tensile and fatigue testing. The dimensions of the fatigue test samples are shown in fig 4.4. After machining , the gage length of the fatigue samples was polished with 4/0 emery paper.

4.4 Mechanical Testing

4.4.1 Tensile Testing

Tensile Tests were done at a constant strain rate of $2 \times 10^{-3} \text{ s}^{-1}$ under stroke control on a closed loop servo-hydraulic Materials Test System. A 25 mm extensometer was used to measure strain. Three tests were conducted for each condition to ensure reproducibility of results. Percentage elongation was calculated for a 30 mm gauge length.

4.4.2 Testing for HCF

Room Temperature HCF tests were carried out under load control in pull-push loading on MTS 810 testing machine. All HCF testing were carried out using a sine wave load cycle at a frequency of 10 Hz. The endurance limit was taken as the stress level corresponding to no failure after 2 million cycles.

4.4.3 Testing for LCF

Room temperature constant amplitude LCF tests under total strain control were performed in air on a 10 T closed loop servo-hydraulic Materials Test System MTS 810). A ramp (triangular) strain wave form with zero mean strain at a constant strain rate of $2 \times 10^{-3} \text{ s}^{-1}$ was used. The LCF tests were continued till fracture. A 25 mm extensometer (Model No 632.11c-20) was used to measure and control strain. Multiple step tests were conducted to obtain the cyclic stress-strain curves. The stress values after about 25 cycles at a constant strain amplitude were recorded. Stabilized hysteresis loops were recorded using X-Y recorder, MTS 431. Plastic strain amplitude was measured from the strain range at zero stress as shown in fig 4.5.

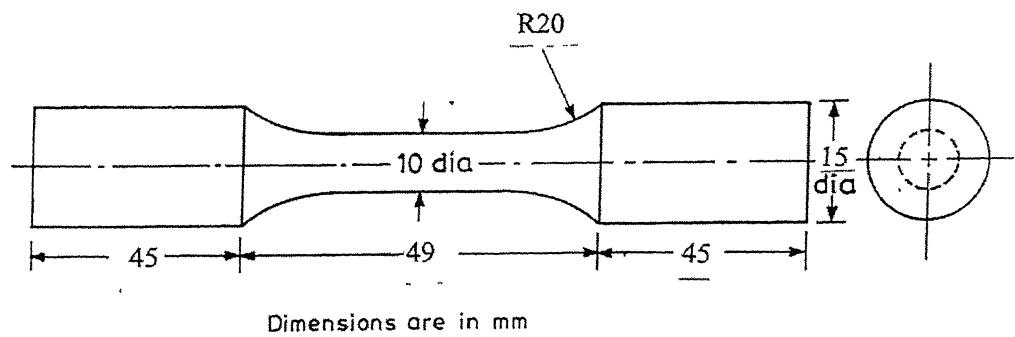


Figure 4.4 The dimensions of the fatigue test samples used in the present investigation.

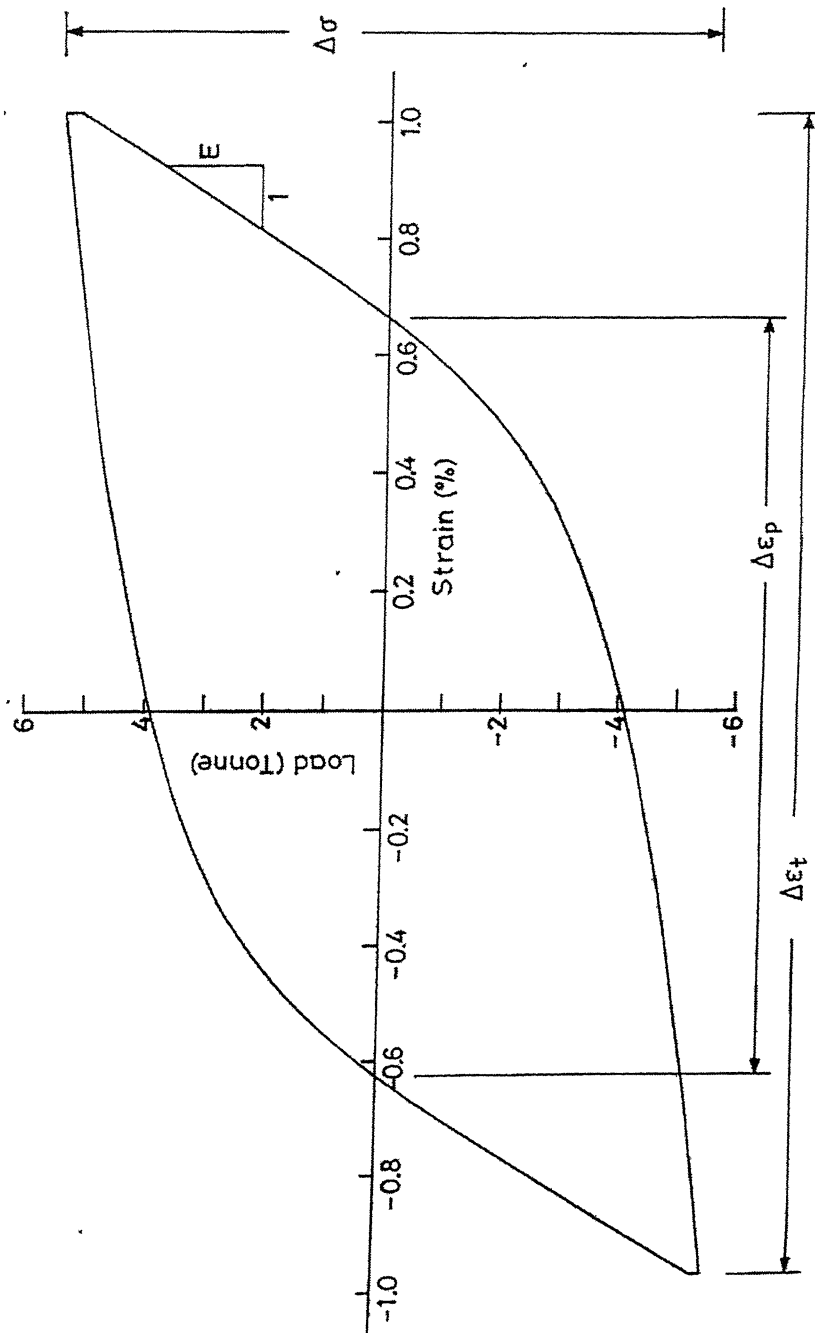


Figure 4.5 A typical hysteresis loop obtained in a strain controlled test used to measure the total and plastic strain amplitudes.

4.4.4 Hardness Testing

(a) Rockwell Hardness. Rockwell hardness was measured using “Indentec Digital Tester” on 150 Kgf load using triangular indenter. Hardness was measured by taking hardness at 7-8 places at center as well as at periphery of the specimen.

(b) Vickers’ Microhardness. The hardness of various phases was measured using a Leitz mini-load microhardness tester. Microhardness was measured using the etched samples for microscopy using 0.49 N load. Microhardness measurements were done in 5-6 different grains for reproducibility. Average of both the diagonals of the indentation was converted to the corresponding HV.

4.4.5 Data Analysis

The Data analysis throughout this investigation was done using spreadsheet software EXCEL that allows both linear & non- linear regression & statistical analysis.

4.5 Metallographic Examination

4.5.1 Sample Preparation

From the rolled samples, 15 mm diameter samples were machined out for microscopic examination. One of the samples was taken along the rolling direction(longitudinal). This sample was obtained by cutting the sample into two halves across the cross section. Second sample was taken perpendicular (cross) to the rolling direction. A minimum of three such samples were examined for each schedules i.e. TMP-1 to TMP-6. Prior to the observation, all the samples were mechanically polished on the emery papers (0 to 4 grades) followed by wheel polishing with alumina powders. The samples were then etched with 3% Nital reagent (3% HNO₃ + 97 % Methanol).

4.5.2 Optical Metallography

Optical Microscopy was carried out using a Leitz Optical Microscope.

4.5.3 Scanning Electron Microscopy

Scanning Electron Microscopy was done under a JEOL-JSM 840A Scanning Electron Microscope. The samples were observed at 15 KV using secondary electron radiation (SE Mode).

4.5.4 Quantitative Metallography

(a) Inter-lamellar Spacing Measurement. The mean inter-lamellar spacing λ , was calculated from the SEM micrographs using the relation

$$\lambda = 1/(2n) \quad (4.1)$$

Where n is the no. of cementite platelets per unit length of secant.

(b) Grain Size Measurement. Grain size of ferrite & pearlite colony size was measured using the linear intercept method described in ASTM E-112.

(c) Image Analyzer. The ferrite aspect ratio, ferrite grain size, volume fraction of ferrite & pearlite was measured at several points on the center and periphery of the specimen using “Image Pro 4.1 Image Analyzer” System. In this system a digital camera is mounted on the top of optical microscope. The micrograph is captured by the camera and the digital picture is fed to the computer software which prepare a pixel map of the picture. Thereafter, using the software and stereological principals various parameters as described above can be calculated.

Results and Discussion

5.1 Effect of thermomechanical Processing of 38MnSiVS5 on its Microstructural Evolution

As mentioned in Chapter 4, a total of 6 thermomechanical processing schedules were given to 38MnSiVS5 steel. The details of these schedules are given in 4.2.2.

In all the six conditions of thermo-mechanical processing, as followed in the present study, the phases present in the steel were (a) polygonal ferrite (free-ferrite) and (b) pearlite. However, volume fraction of these phases was found to be different in differently processed conditions. The interlamellar spacing in pearlite was also found to be slightly affected by thermomechanical processing schedules. For the sake of the microstructural classification of different TMPs the structures have been designated as (a) polygonal ferrite – fine pearlite (PF/FP), (b) polygonal ferrite – medium pearlite (PF/MF) and (c) polygonal ferrite – coarse pearlite (PF/CP). While TMP1 (i.e. finished rolling temp 800°C) resulted in PF/FP microstructure, TMP2 (finish rolled at 900°C) and TMP3 (finish rolled at 1000°C) yielded a PF/MP and PF/CP microstructures respectively. The optical micrographs of above 3 conditions are shown in fig 5.1 and fig. 5.2 in cross (normal to rolling) and longitudinal (in the plane of rolling) directions respectively. Whereas, the SEM micrographs in cross and longitudinal directions are shown in fig. 5.3 and fig. 5.4 respectively.

As described in Chapter 4, volume fraction of polygonal ferrite (free ferrite that was not part of pearlite), ferrite grain size, pearlite inter lamellar spacing and the aspect ratio of proeutectoid ferrite in differently processed steels was measured by the quantitative metallography technique. Values obtained for these different microstructural parameters in the cross (normal to rolling direction) as well as longitudinal (in the plane of rolling) directions of the specimen are given in Table 5.1 and 5.2 respectively. There was not much of the variation in pearlite colony size. It was found to be varying between 8-12 μ meter in all the three structures.

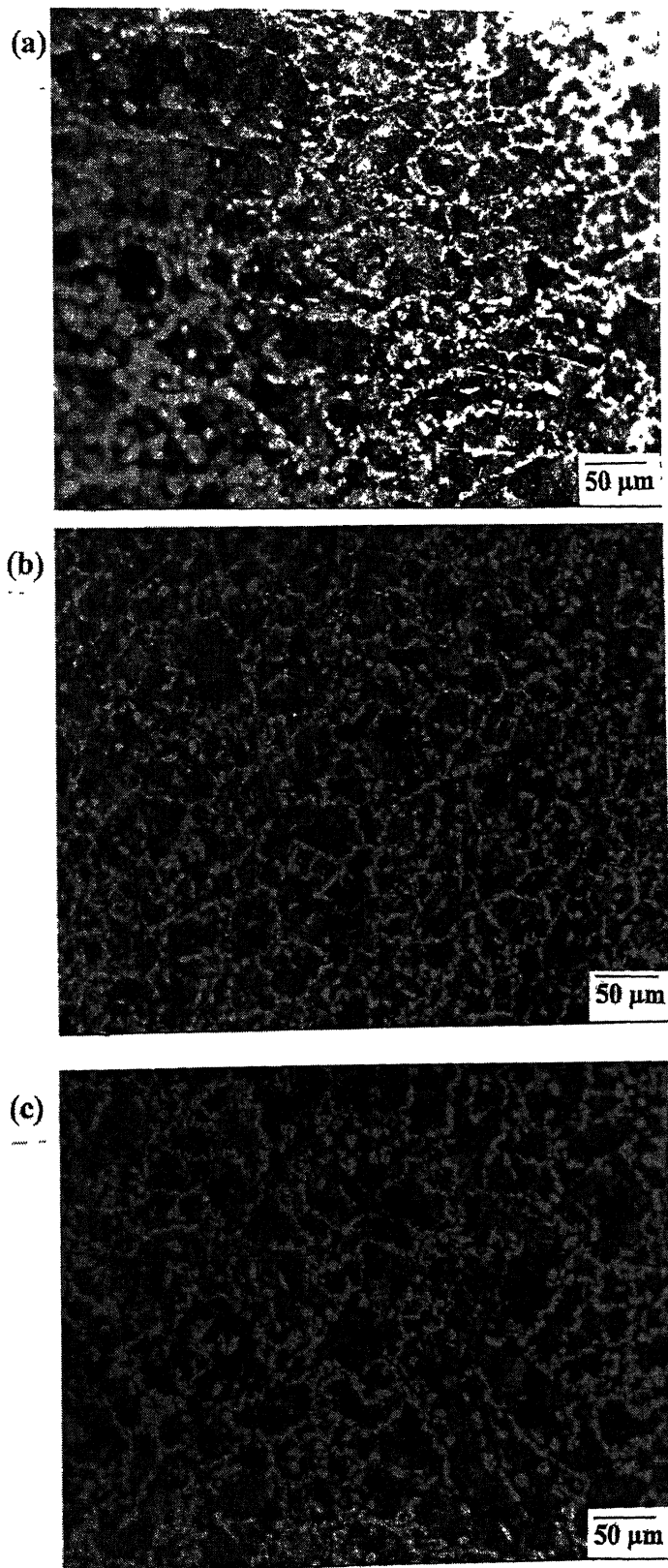


Figure 5.1 The optical micrographs of 3 TMP conditions in cross(normal to rolling)direction (a) TMP1(PF/FP) (b) TMP2(PF/MP) (c) TMP3 (PF/CP).

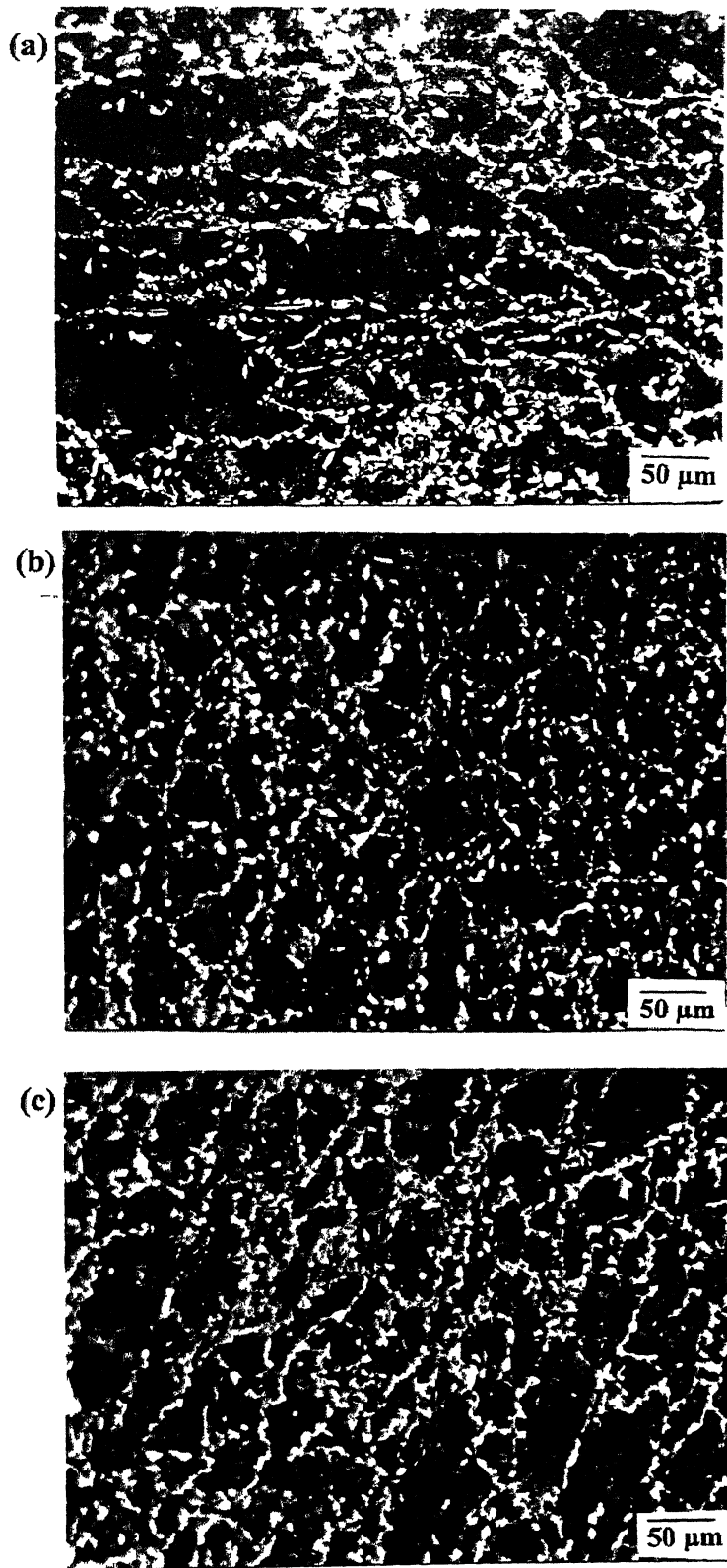


Figure 5.2 The optical micrographs of 3 TMP conditions in longitudinal (in the plane of rolling) direction (a) TMP1(PF/FP) (b) TMP2(PF/MP) (c) TMP3 (PF/CP).

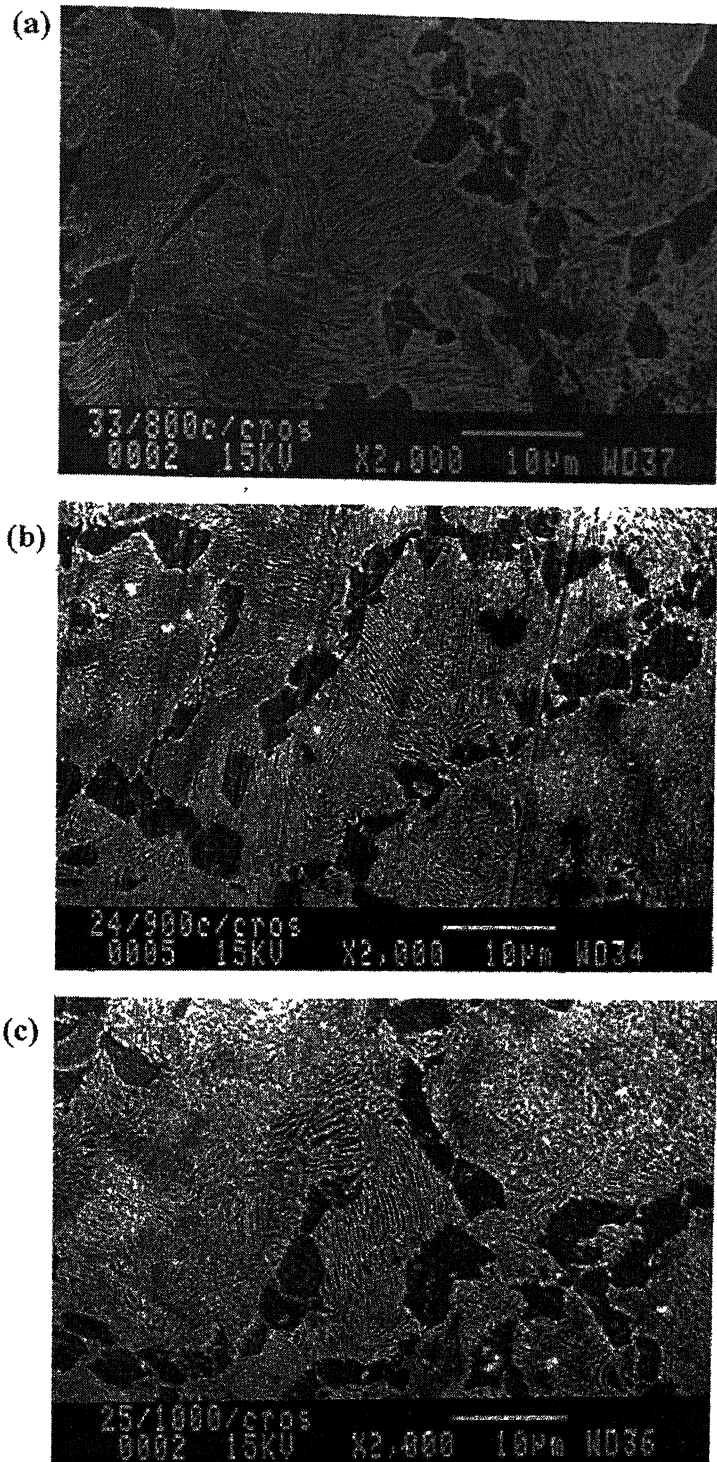


Figure 5.3 The SEM micrographs of 3 TMP conditions in cross(normal to rolling)direction (a) TMP1(PF/FP) (b) TMP2(PF/MP) (c) TMP3 (PF/CP).

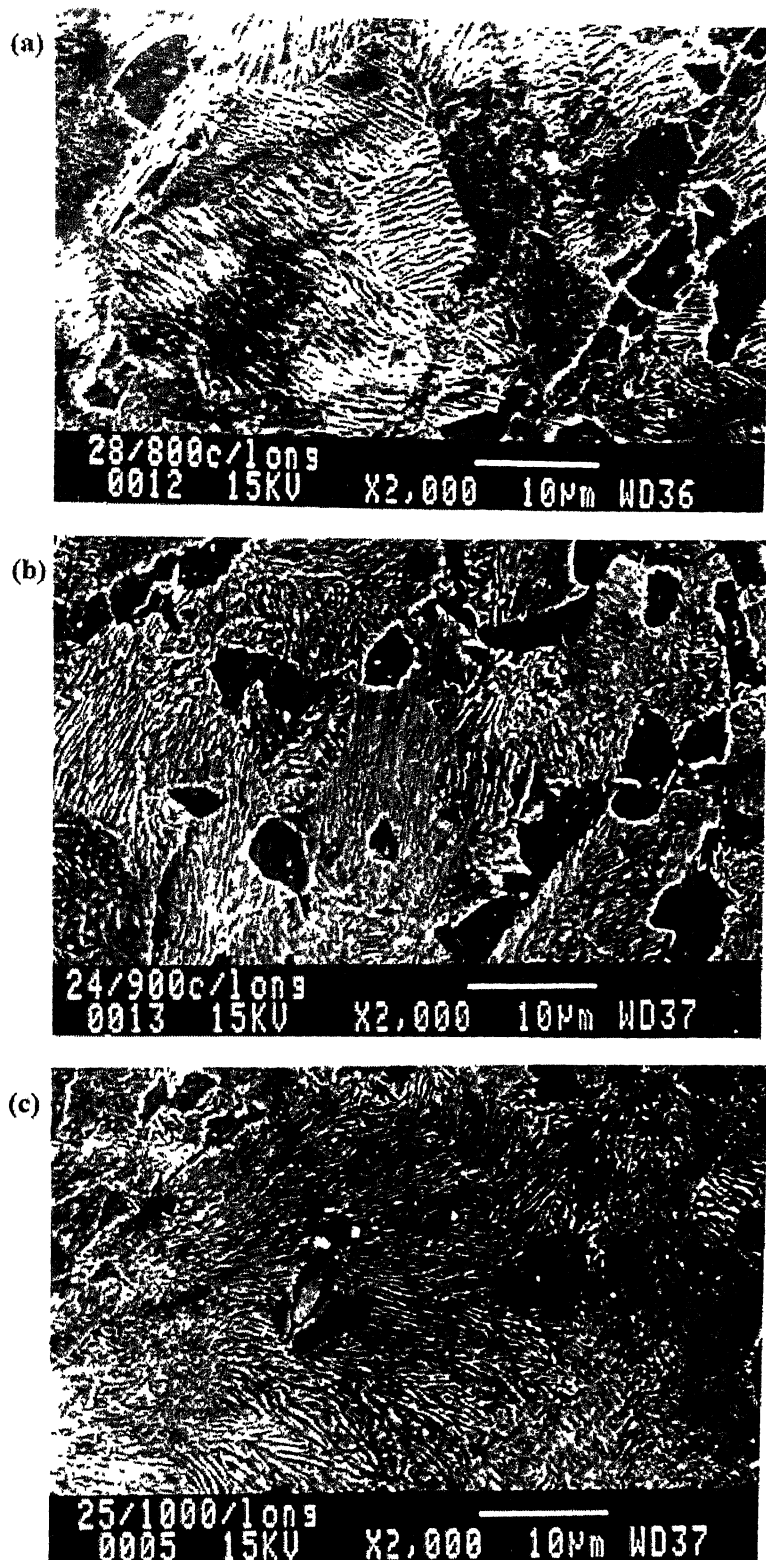


Figure 5.4 The SEM micrographs of 3 TMP conditions in longitudinal(in the plane of rolling)direction (a) TMP1(PF/FP) (b) TMP2(PF/MP) (c) TMP3 (PF/CP).

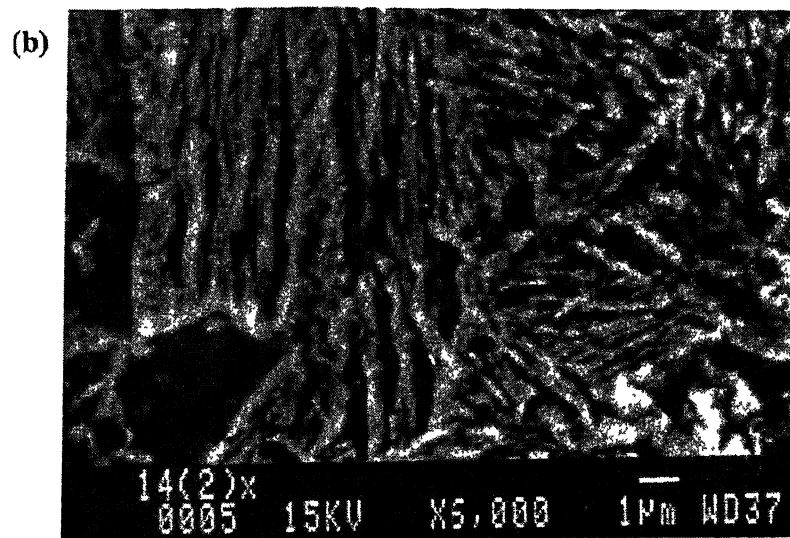
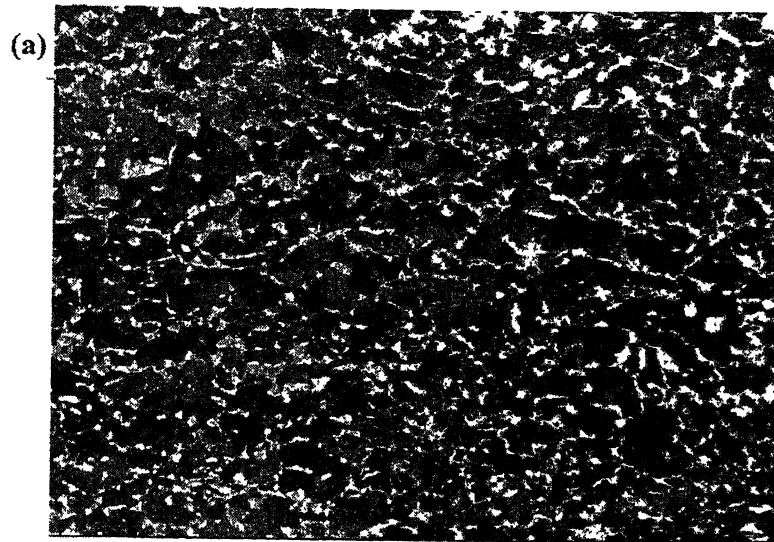


Figure 5.5 The optical and SEM micrographs of TMP6 condition
(a) Optical (b)SEM.

Typical optical & SEM micrographs of the steel processed through TMP6 are shown in fig 5.5. Microstructures obtained in the steel processed through TMP4 and TMP5 were similar and had no significant differences as measured by preliminary examination by quantitative metallography techniques. No detailed examination was therefore carried out on these samples. However, it can be seen that these conditions also resulted in polygonal ferrite - pearlite microstructure. A comparison of pearlitic spacing in them indicated that they will be close to PF/MP microstructural state

Table 5.1 Microstructural Properties of 38MnSiVS5 in normal to rolling direction (i.e. in Cross direction).

Condition	Ferrite Volume Fraction (In %)		Ferrite Aspect Ratio		Ferrite Grain Size (in μ meter)		Inter Lamellar Spacing(in μ meter)	
	At Periphery	At Center	At Periphery	At Center	At Periphery	At Center	At Periphery	At Center
PF/CP	36	35	2.06	1.98	7.0	7.2	0.17	0.19
PF/MP	30	29	1.95	1.94	5.8	6.0	0.15	0.17
PF/FP	26	24	1.89	1.85	5.2	5.4	0.11	0.12
As Recd	37	36	1.96	1.90	7.5	8.2	0.24	0.26

Table 5.2 Microstructural Properties of 38MnSiVS5 in the plane of rolling (i.e. in Longitudinal direction).

Condition	Ferrite Volume Fraction (In %)		Ferrite Aspect Ratio		Ferrite Grain Size (in μ meter)		Inter Lamellar Spacing(in μ meter)	
	At Periphery	At Center	At Periphery	At Center	At Periphery	At Center	At Periphery	At Center
PF/CP	36	34	2.1	2.05	6.5	7.0	0.18	0.20
PF/MP	31	29	1.97	1.95	5.8	6.2	0.16	0.18
PF/FP	29	26	1.87	1.85	5.6	5.9	0.12	0.14
As Recd	37	36	1.95	1.85	7.5	8.2	0.25	0.26

5.1.1 Effect on ferrite-pearlite volume fraction

As shown in Table 5.1 Table 5.2, the volume fraction of free-ferrite increased as the finishing rolling temperature increased [in case of TMP3 (PF/CP) as compared to TMP1 (PF/FP)]. This change in free-ferrite volume fraction in steel can be explained with the help of the CCT diagram of the 38MnSiVS5 steel, as shown in fig 5.6(a).

The thermomechanical process of microalloyed steels is characterized by a complex interaction between different processes occurring in the material, such as dynamic recovery and dynamic recrystallization of austenite grains as well as dynamic precipitation of carbides and/or carbonitrides. Since 38MnSiVS5 steel contains vanadium as a micro-alloying element, deformation induced precipitation of very fine carbides and/or carbonitrides of vanadium is expected to play the decisive role by retarding the dynamic recrystallization during thermomechanical rolling [Meyer et al.]. As the temperature drops during rolling, the super saturation of microalloying elements in the austenite increases. The deformation under falling finishing temperature conditions, therefore, can lead to the dynamic precipitation of vanadium

temperature conditions, therefore, can lead to the dynamic precipitation of vanadium carbides/ carbonitrides. If there is adequate super saturation of microalloying element as well as carbon or nitrogen in the austenite the recrystallization that may take place during rolling is heavily impaired by deformation induced precipitation. Therefore the recrystallization temperature of 38MnSiVS5 is about 900°C. Fig. 5.6(b) offers a schematic representation of the marked acceleration and recrystallization [Meyer et al.]. The blocking of recrystallization ensures that there is a formation of virgin grain only with the γ/α -transformation. Therefore, the shifting of TTT curve to the left leads to more pearlite formation in TMP1 (PF/FP) case.

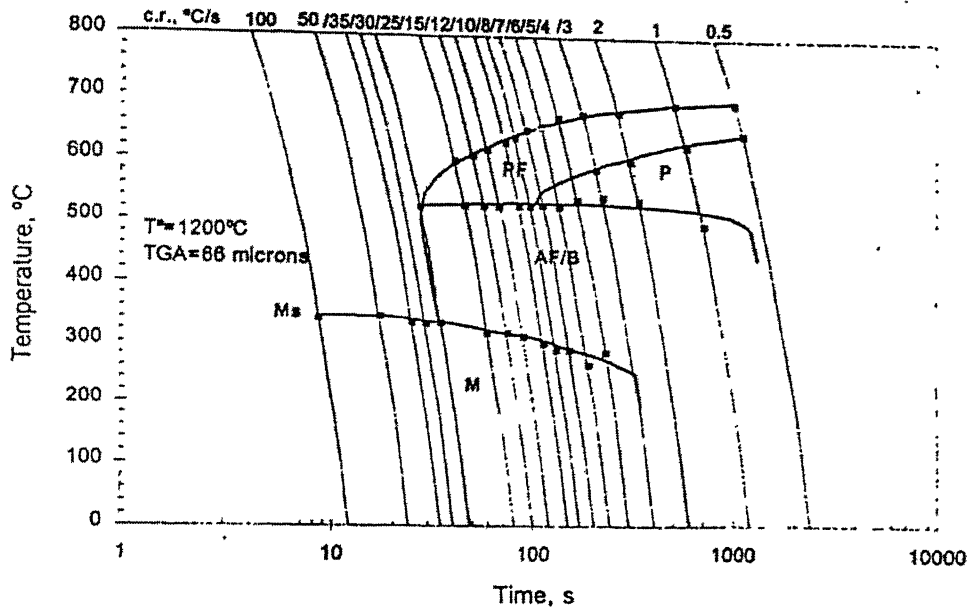
5.1.2 Effect on Inter-lamellar spacing of pearlite

As shown in table 5.1 & 5.2 the inter-lamellar spacing was minimum in case of TMP1 (PF/FP) condition. This may be due to relatively faster cooling rate in case of TMP1 than other two conditions. It was observed that there was marked decrease in inter-lamellar spacing (about 50%) as compared to as received sample. However, variation of inter lamellar spacing among three TMP conditions were not much.

5.1.3 Effect on Ferrite Grain Size

The ferrite grain size was finer in case of TMP1 than other two conditions. The transformation kinetics are especially influenced by the microalloying elements during thermomechanical processing. Whereas elements in solid solution lead to a retarded transformation, carbonitrides in the austenite result in an acceleration because of their nucleation. An especially marked acceleration of transformation occur if deformation-induced fine precipitates block the recrystallization of the austenite & the transformation of an austenite with a very high defect density occurs during thermomechanical processing. The transformation acceleration increases as the rolling temperature drops & the degree of deformation increases. Therefore, due to relatively fast cooling in TMP1 the resultant ferrite grain size is finer than other two microstructure.

(a)



(b)

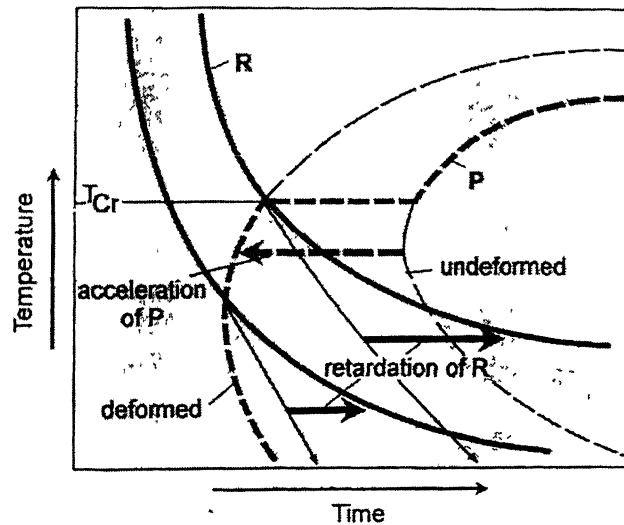


Figure 5.6 (a) Continuous cooling transformation (CCT) diagram after austenitization at 1200°C. (b) Interaction of recrystallization R and precipitation P.

5.2 Effect of Thermomechanical Processing of 38MnSiVS5 on its Tensile Properties

The engineering stress-strain plots for the as-received material as well as material having three different microstructures obtained through TMP1 – TMP3 are shown in Fig. 5.7. It can be seen that the yield point phenomenon, indicative of Lüders' band propagation, was present in TMP-2 & TMP-3 conditions. The tensile properties of 38MnSiVS5 steel in different conditions, namely 0.2% Yield Strength, Young's modulus, Ultimate Tensile Strength (UTS), % tensile elongation, % reduction in area, strength coefficient (K) and strain hardening exponent (n) (in the constitutive relationship $\sigma = K\epsilon^n$) are given in Table 5.3.

It is seen that the modulus of the steel remains unaffected, as expected, by its thermomechanical processing. Further, while the monotonic 0.2% yield strength of PF/FP and PF/MP was nearly the same, that of PF/CP was lower in comparison. In contrast, the steel in its as-received state had the lowest 0.2% yield strength among all the four conditions. Similarly, the UTS of the steel increased monotonically from the PF/CP state to PF/FP state. On the other hand, percentage tensile elongation as well as the percentage reduction in area at fracture decreased with decreasing finish rolling temperature. It should also be noted that the strain hardening coefficient, n, of 38MnSiVS5 steel was also influenced by its thermomechanical processing and increased monotonically from the value of 0.30 (PF/FP) to 0.32 (PF/CP). These trends in variation of mechanical properties thermomechanically treated steel can be explained as under.

As discussed earlier, the driving force for heterogeneous precipitation of V(C,N) increases with decrease of finish rolling temperature, it is more for the PF/FP structure due to the lower finishing temperature (800°C) for samples treated through TMP. This leads to the precipitation of more numerous and finer V(C,N) particles in the PF/FP structure compared with the PF/CP condition. These precipitates form in free polygonal ferrite as well as the in the interlamellar ferrite of pearlite. Further, PF/FP condition of the steel was also found to contain a higher volume fraction of pearlite (Tables 5.1, 5.2). The higher volume fraction of pearlite as well as finer and numerous precipitation in ferrite cause the strengthening of the steel under PF/FP condition obtained by TMP1. Both the above factors are also responsible for lowering the

ductility and hence the ductility was found to be the highest in PF/CP condition and lowest in PF/FP condition.

Also, in theory the uniform true strain, ϵ_u , is equal to the strain hardening exponent, n . Investigations on fully pearlite steels with varying inter-lamellar spacing have revealed that the strain hardening exponent decreased with decreasing inter-lamellar spacing in that class of steels also [Sunwoo et al., 1982; Dollar et al. 1988]. The strain hardening exponent of steel, as obtained in the present investigation, was lowest for the PF/FP condition (TMP1) which had the highest volume fraction of pearlite and the finest inter-lamellar spacing. The strength coefficient, K , is seen to increase with decreasing inter-lamellar spacing and this observation is also consistent with earlier findings.

The processes occurring in microalloyed steel during hot rolling are the basic reason why the rolling temperature influences microstructural changes. This in turn leads to a corresponding dependence of yield strength on rolling temperature. As the rolling temperature drops, the thermomechanical effect is intensified initially, so an increase in yield strength results – mainly because of grain refinement. The precipitation hardening of the ferrite reaches a maximum, for as the rolling temperature drops further, the deformation induced precipitation of the microalloying elements in the austenite increases and the remaining alloying fraction for precipitation hardening decreases accordingly. Finally, a further drop in the rolling temperature leads to a deformation that can no longer be compensated by the recrystallisation and results in a corresponding strengthening. The UTS is more in TMP1 due to finer grains size of ferrite & more percentage of pearlite as compared to TMP2 and TMP3.

Since the volume fraction of pearlite in case of PF/FP state of steel is higher, more carbon atoms are used in the formation of cementite, relatively less carbon atoms are left in the Cottrell atmosphere to resist the dislocation movement. The extent of the yield point phenomenon was therefore found to be weaker in the PF/FP state (TMP1) than in PF/MP (TMP2) and PF/CP (TMP3) states. We can also observe that the difference in UTS is more marked than difference in 0.2% yield strength in case of TMP1(PF/FP) when compared with the as received or TMP3 conditions.

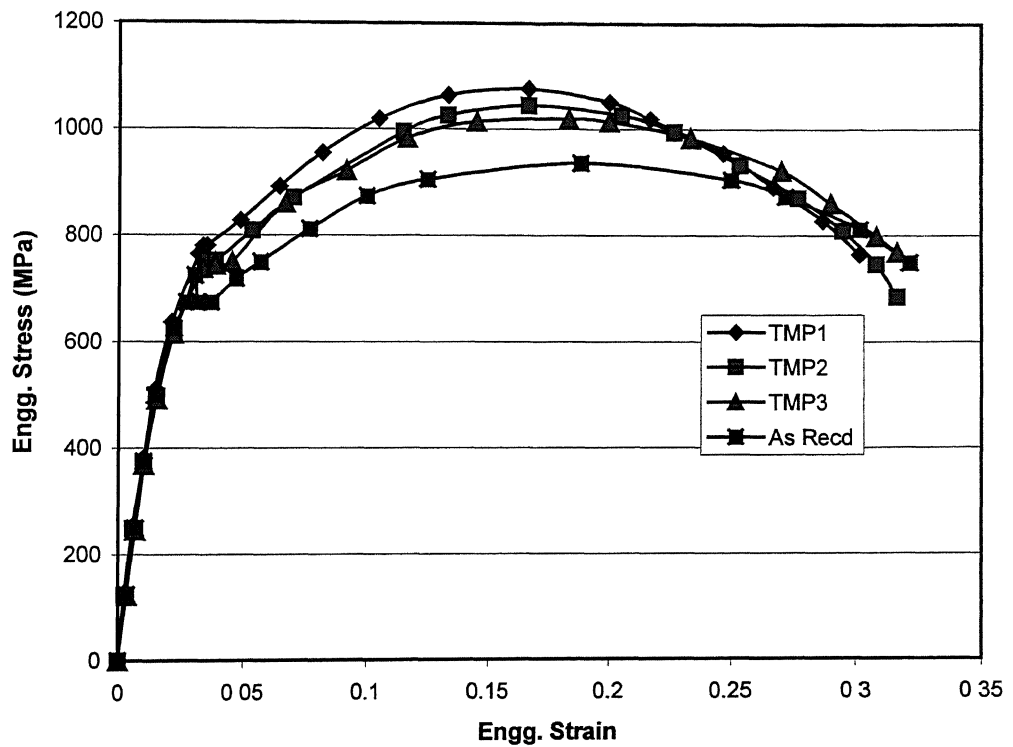


Figure 5.7 Monotonic engineering stress – strain curve for the three different TMP conditions as well as-received material.

Table 5.3 Room temperature tensile properties of 38MnSiVS5

Mechanical Properties	As Received	TMP1 (PF/FP)	TMP2 (PF/MP)	TM3 (PF/CP)
0.2% Yield Strength (MPa)	724 (Upper) 674 (Lower)	780	752	749
Young's Modulus (GPa)	210	215	210	210
Ultimate Tensile Strength (MPa)	936	1076	1044	1019
% Elongation	34.4	25.9	27.6	30.2
% Reduction in Area	57.8	53.8	56.7	57.7
Strength Coefficient, K (MPa)	1940	2268	2219	2214
Strain Hardening Coefficient, n	0.30	0.30	0.32	0.33

5.3 Effect of thermomechanical processing of 38MnSiVS5 on its hardness.

The Rockwell hardness was measured using the digital tester “indentec”. Vickers’s microhardness was carried out using 0.49 N load . The values are given in table 5.3. The difference may be attributed to different ferrite volume fraction and microstructures in three conditions.

Table 5.4 Hardness of Three microstructures and as received sample.

Condition	Rockwell hardness (HRC)	Vickers microhardness (HV)
TMP1	29-31	295-310
TMP2	27-29	282-290
TMP3	25-27	260-280
As Received	24-26	260-275

5.4 Effect of Thermomechanical Processing on LCF Behavior

5.4.1 Cyclic Stress Response

The cyclic stress response for steel processed through all six thermomechanical processing schedules was examined. However, due to similar trend and morphology in TMP4-TMP6 conditions, further quantitative analysis was focused only on TMP1-TMP3 conditions. The general trends were that the number of cycles to failure decreased with increase in the applied strain in all the conditions. The details of the cyclic stress response is given in the subsequent paragraphs below

5.4.1.1 TMP1 (Polygonal Ferrite/Fine Pearlite)

The peak tensile stress versus the number of cycles relationship for a fixed total strain amplitude in the range of 0.4% to 1.2% is given in Fig. 5.8. In this condition, at total strain amplitudes greater than 0.8%, cyclic hardening was observed throughout the cyclic loading. However, rate of hardening increased as the strain was increased. Maximum cyclic hardening was observed in 1.2% strain case. At a total strain amplitude less than 0.8%, cyclic softening was present for initial 8-10 cycles followed by steady state response for the rest of the life. At total strain amplitudes of 0.8% a stable response was seen for initial 8-10 cycles followed by cyclic hardening.

5.4.1.2 TMP2 (Polygonal Ferrite/Medium Pearlite)

The response was same as that of TMP1, whereas degree of hardening was more than that of TMP1 but less than TMP3. The no of cycles to failure were more in this case as compared to TMP1 for the same amount of applied strain. The peak tensile stress versus the number of cycles relationship for a fixed total strain amplitude in the range of 0.4% to 1.2% is given in Fig. 5.9 for TMP2 condition.

5.4.1.3 TMP3 (Polygonal Ferrite/Coarse Pearlite)

The variation of peak tensile stress with the number of cycles for different strain amplitudes for the PF/CP microstructure is shown in Fig. 5.10. At total strain amplitudes greater than 1.0%, very strong hardening was observed throughout the loading cycle. For total strain amplitude of greater than 0.8% and up to 1.0%

stabilized response was observed for initial 6-8 cycles followed by cyclic hardening till about mid life, thereafter, steady state behavior was observed up to failure. For strain amplitudes of 0.6 to 0.8%, cyclic softening was noticed for initial 6-8 cycles followed by cyclic hardening for about 100 cycles, there after, steady state behavior was seen till failure. For strain amplitudes less than 0.6% cyclic hardening was observed for initial few cycles (8-10 cycles) followed by softening till about 100 cycles, thereafter, steady state behavior was seen till failure at about 5000-6000 cycles.

The cyclic response of an eutectoid carbon steel as a function of inter-lamellar spacing was investigated by Sunwoo et al. (1982). Cyclic softening was observed in fine pearlite and cyclic hardening was seen in coarse pearlite. A Tendency to cyclically harden as the strain amplitude was increased could be observed in medium spaced pearlite and also in as-forged microalloyed steel [Sarma, 1998; Yang and Fetemi, 1995].

When dislocation density increases with plastic work, the flow stress may decrease due to an increase in the density of mobile dislocations but it may also increase due to a decrease in dislocation mobility arising out of dislocation pile up/forest formation. It has been suggested that cyclic softening is the result of formation and spreading of dislocation sources along the specimen gauge length in the first few cycles. This spreading continues until the dislocation sources cover the whole gauge volume of the specimen [Roven and Nes, 1991; Pohl, Mayr and Macherauch, 1981; Suresh, 1991]. The unpinning of the dislocations from the atmosphere of solute atoms in the preceding cycle, which makes the dislocations mobile, results in a decrease in the stress amplitude in successive cycles. This phenomenon is to be expected in materials shown in a sharp yield point and yield point elongation, as is the case with the present MA steel for all the microstructural conditions employed. A similar behavior was observed for the as-forged condition by Sarma (1998).

The observed cyclic hardening at higher strain amplitudes is associated with conventional work hardening resulting from the rearrangement of the dislocation structure from walls and labyrinths to cells and sub grains, and from a refinement of these features with increasing plastic strain [Roven and Nes, 1991]. Formation of

these structures results in the stabilization of the cyclic stress response. Hardening would have been greater and more sustained if the dislocation-dislocation interactions were not lowered by cell formation. Moreover, at large strain amplitudes, work hardening resulting from the interactions among dislocations and between dislocations and precipitates dominate over the softening resulting from the generation of mobile dislocations.

5.4.1.4 TMP4-TMP6

The variation of peak tensile stress with the number of cycles for different strain amplitudes for these conditions is shown in Fig. 5.11 to fig. 5.13. The variation is almost similar to the TMP1-TMP3 explained earlier. The detailed examination and investigation were not undertaken due to almost similar morphology in all these conditions.

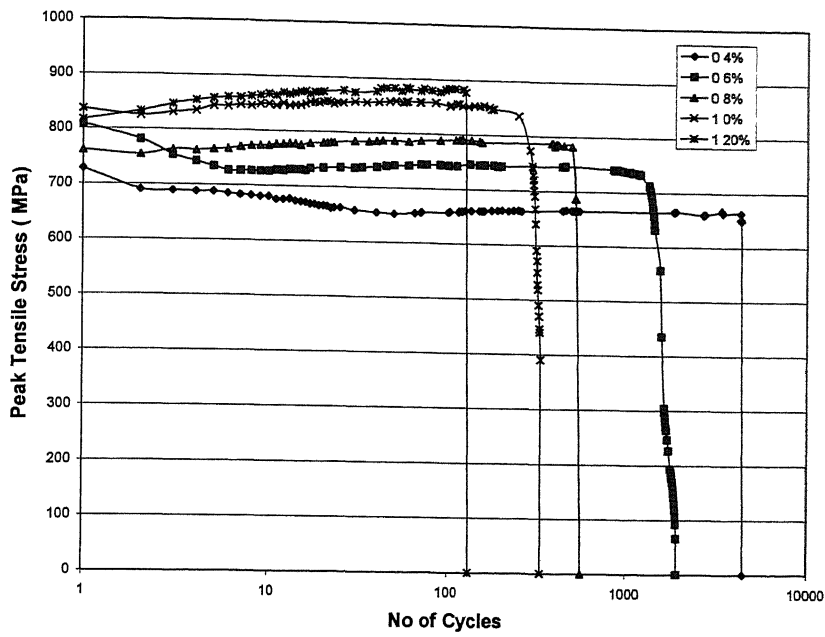


Figure 5.8 Cyclic stress response of the TMP1(PF/FP)condition at different total strain amplitude.

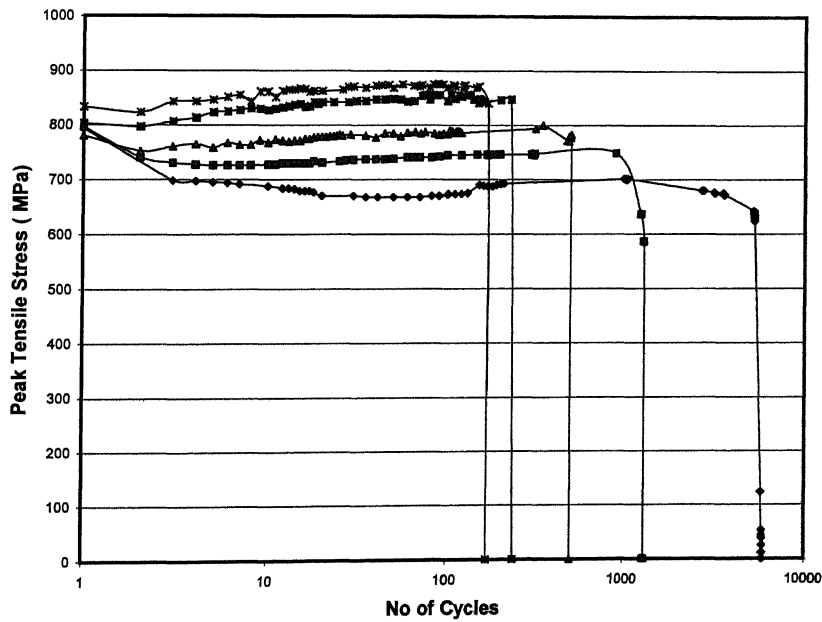


Figure 5.9 Cyclic stress response of the TMP2 (PF/MP) condition at different total strain amplitude.

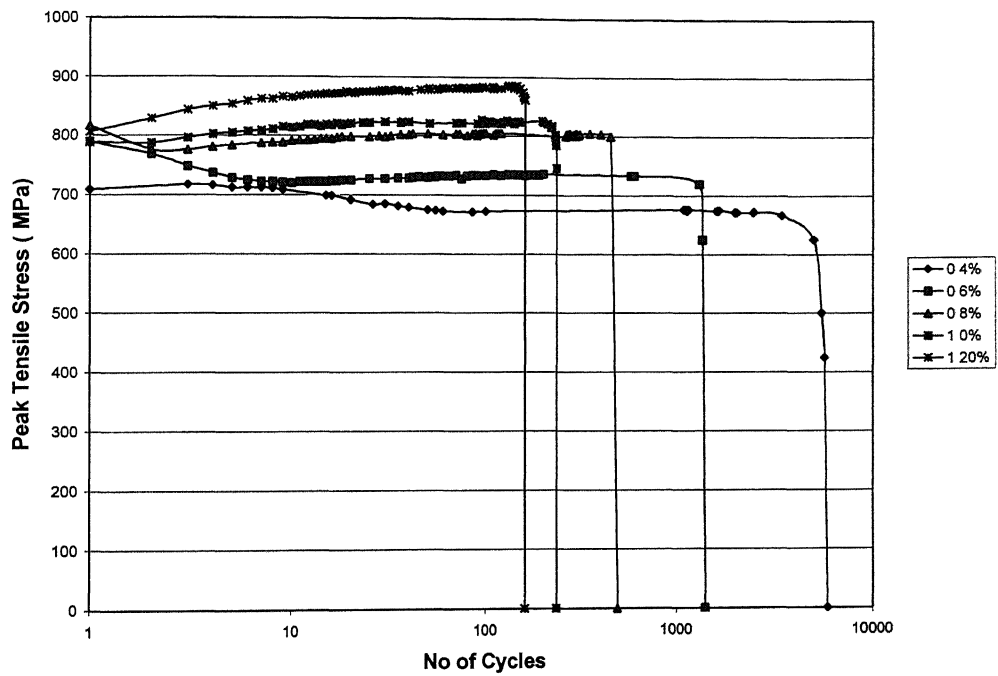


Figure 5.10 Cyclic stress response of the TMP3(PF/CP)condition at different total strain amplitude.

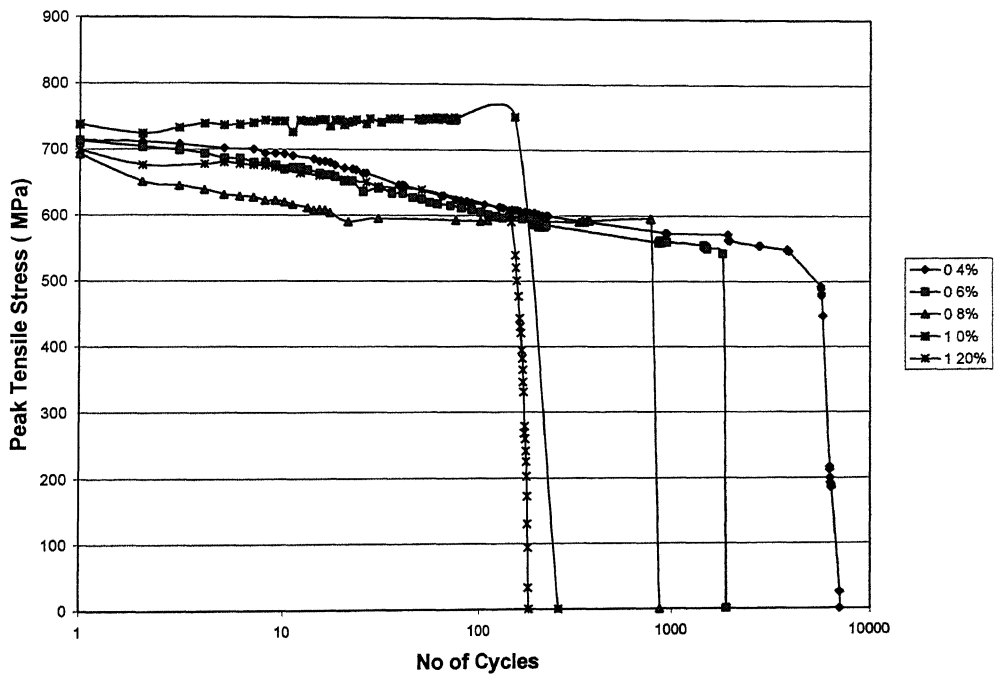


Figure 5.11 Cyclic stress response of the TMP4 condition at different total strain amplitude.

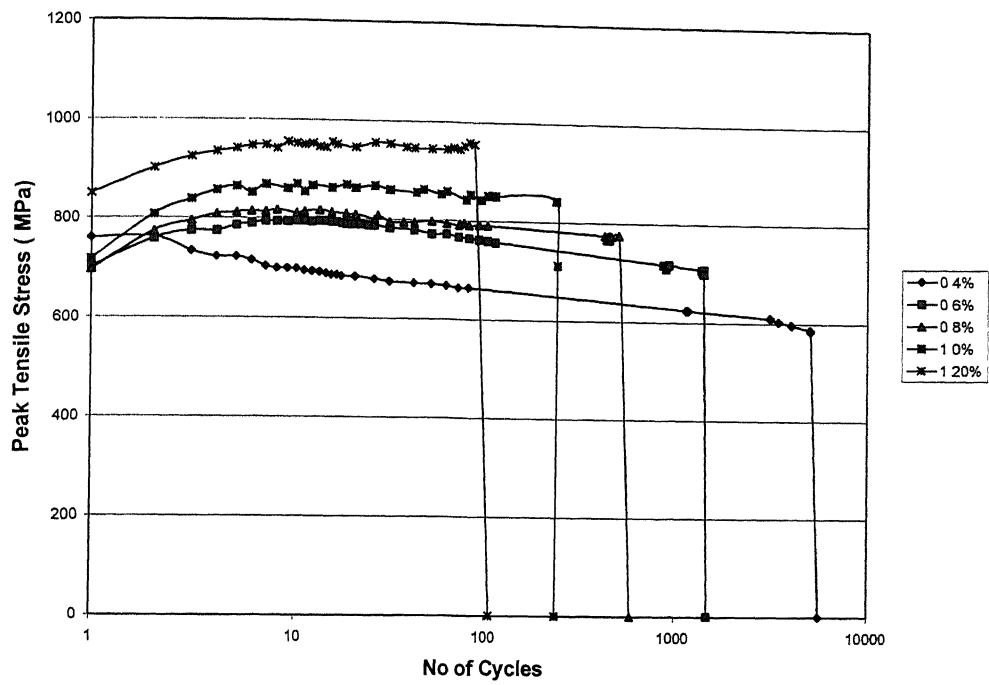


Figure 5.12 Cyclic stress response of the TMP5 condition at different total strain amplitude.

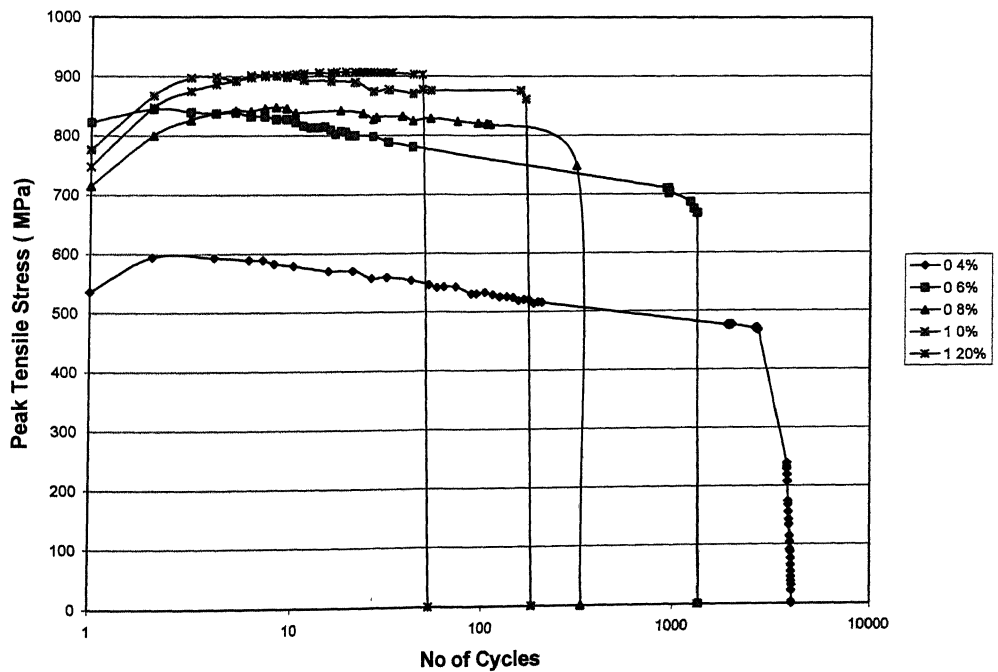


Figure 5.13 Cyclic stress response of the TMP6 condition at different total strain amplitude.

5.4.2 Cyclic Stress – Strain Curve

The stabilized stress or the stress at half-life (in case stress was not stabilised), obtained by-constant amplitude total strain controlled tests was used to plot the cyclic stress-strain (CSS) curves for the three microstructural conditions in Fig. 5.14. The data was fitted to the well-known power law.

$$\frac{\Delta\sigma}{2} = K' \left(\frac{\Delta\varepsilon_p}{2} \right)^{n'} \quad (5.1)$$

The correlation between the experimental points and the predicted relationship was satisfactory. The cyclic strain hardening exponent, n' , the cyclic strength coefficient, K' , and the correlation coefficient for the three microstructural conditions are given in Table 5.5. Slightly lower value of correlation coefficient is because of experimental scatter and taking the values of plastic strain at half life instead of stabilized stress value in some cases.

Table 5.5 Parameter describing the CSS curves for three microstructural conditions

Condition	n'	K' (MPa)	Correlation coefficient
TMP-1 (PF/FP)	0.3727	5512	0.93
TMP-2 (PF/MP)	0.4303	7061	0.91
TMP-3 (PF/CP)	0.4813	8741	0.88

The CSS curve for the PF/FP microstructure was seen to lie above that for the PF/CP condition, which implies that the PF/FP structure is stronger than other two conditions. This is because of high volume fraction of pearlite, finer ferrite grain size and lower inter – lamellar spacing in case of TMP1 (PF/FP) than other two conditions.

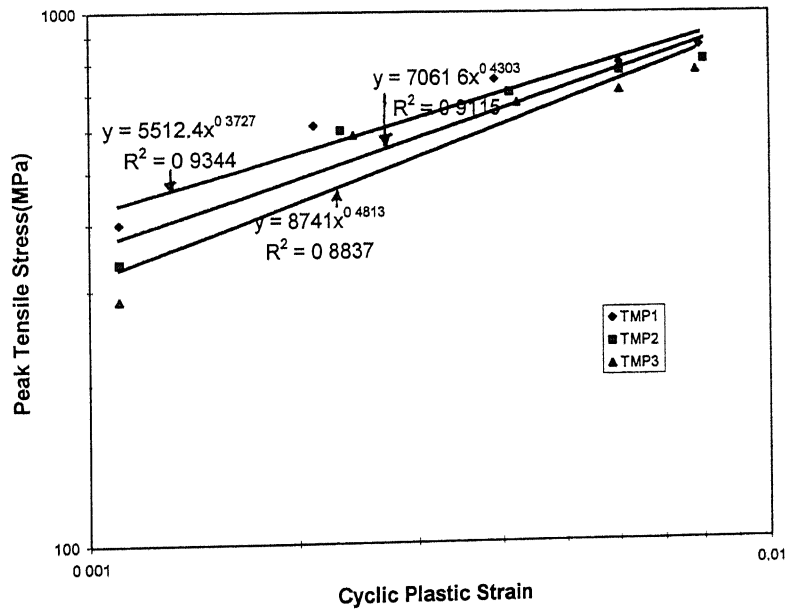


Figure 5.14 Cyclic stress-strain curves for the three microstructural conditions as obtained by constant total strain amplitude controlled tests. Stabilized or half-life stress values were obtained from the stress response curves.

5.4.3 Coffin-Manson and Basquin Plots

The Coffin-Manson law is given by the following relationship

$$\frac{\Delta \varepsilon_p}{2} = \varepsilon'_f (2N_f)^c \quad (5.2)$$

where ε'_f is the fatigue ductility coefficient and c is the fatigue ductility exponent. The logarithm of the plastic strain amplitude, $\Delta \varepsilon_p/2$, was plotted against the logarithm of the number of load reversals to failure, $2N_f$, and a linear relation was obtained for all the three structures (Fig. 5.15). The slope, c , for the TMP1(PF/FP) and TMP2(PF/MP) is almost the same. Whereas, it was more in case of TMP3(PF/CP) indicating that this structure is more ductile than other two conditions. The abscissa, ε'_f , which is a measure of true strain to fracture, for the three microstructures was 0.16, 0.19 and 0.26 respectively, thus indicating more strain required for fracture in case of PF/CP than other two conditions. The fatigue life for the PF/CP condition exceeded that of the PF/FP structure by nearly 35-60% for the same amount of plastic strain at low & high strain amplitudes respectively. Fatigue life for the PF/MP condition was about 15% more than that for the PF/FP structure on the plastic strain basis. However, the fatigue lives of the three microstructures, when seen in terms of the total strain amplitude, turned out to be nearly the same, as shown in Fig. 5.16. The fatigue life is known to depend on plastic strain amplitude. For the same total strain amplitude, the proportion of elastic to plastic strain was observed to be different for different microstructures. This was due to the higher tensile yield strength in the PF/FP as compared with the PF/CP condition. Therefore, the amount of plastic strain induced in the PF/CP condition was more, while that for the PF/FP conditions was less for a fixed total strain amplitude. Hence, fatigue life was the same for a fixed total strain amplitude in case of all the three microstructures but they were different, as stated above, when the comparison was based on constant plastic strain amplitude. In monotonic loading the percentage reduction in area for the PF/CP condition was more than that for the other two structures. Therefore, the fatigue life for the PF/CP structure was significantly more than that for the PF/FP condition. The cyclic ductility

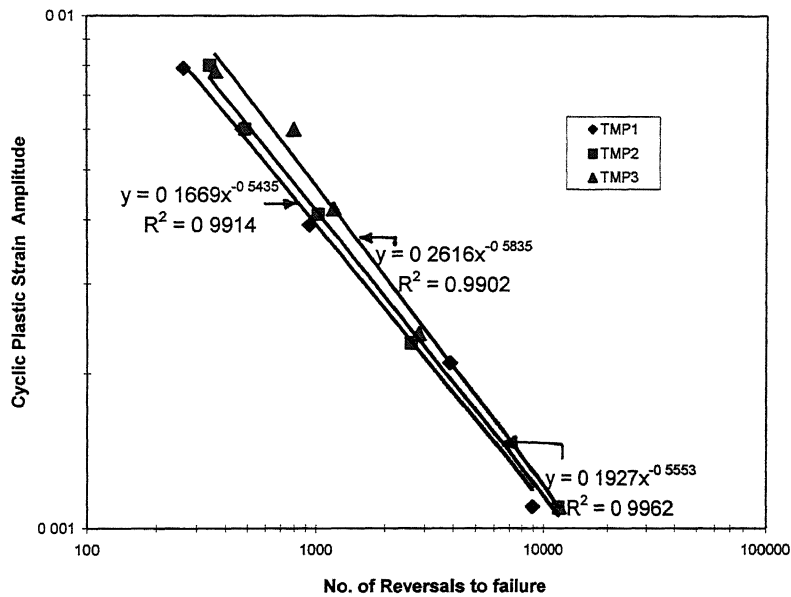


Figure 5.15 Coffin-Manson Plots for the three conditions

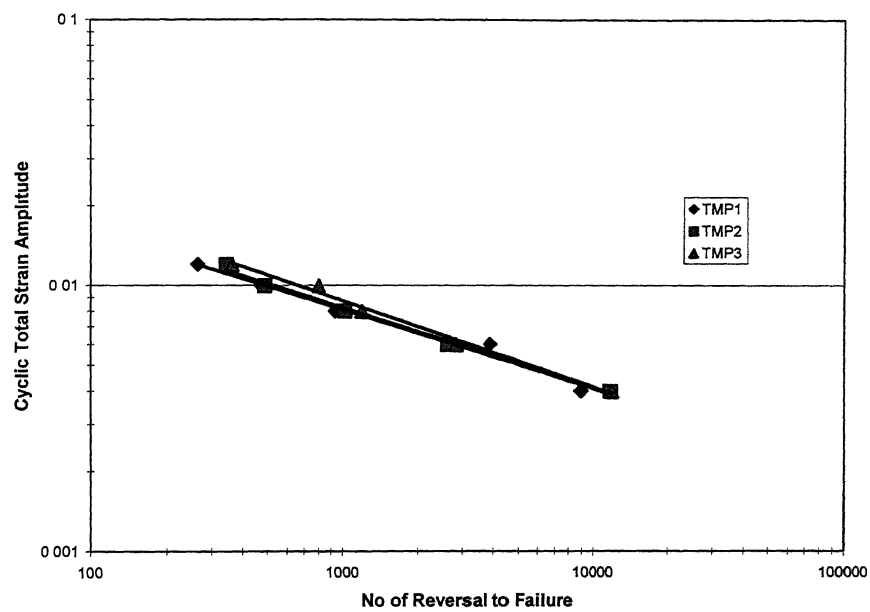


Figure 5.16 Total strain amplitude as a function of reversals to failure for the three TMP conditions.

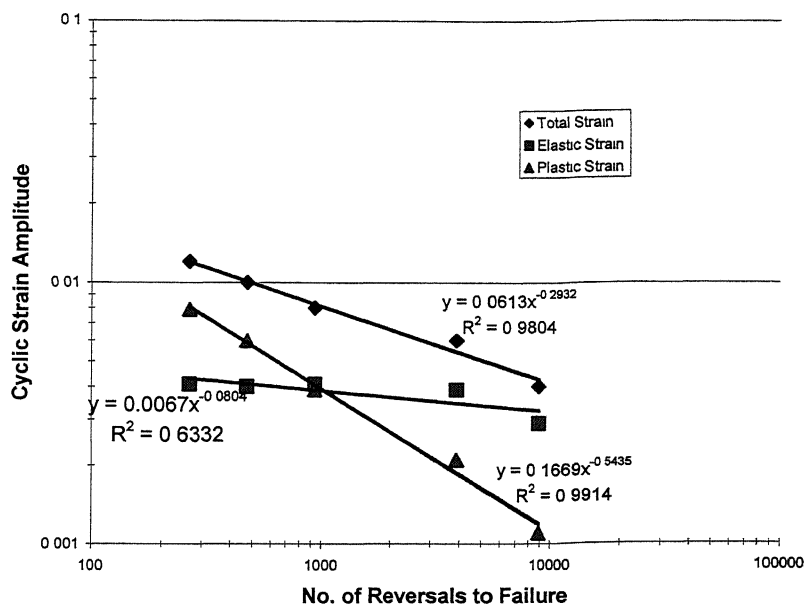
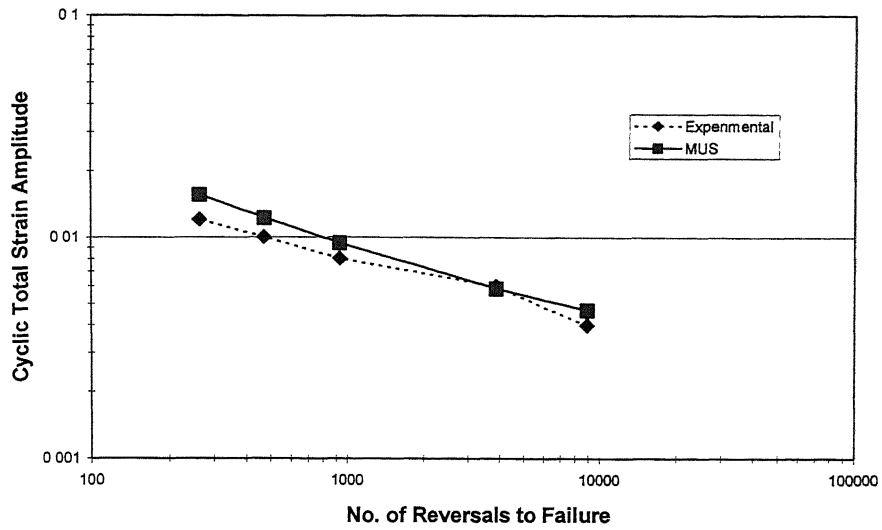
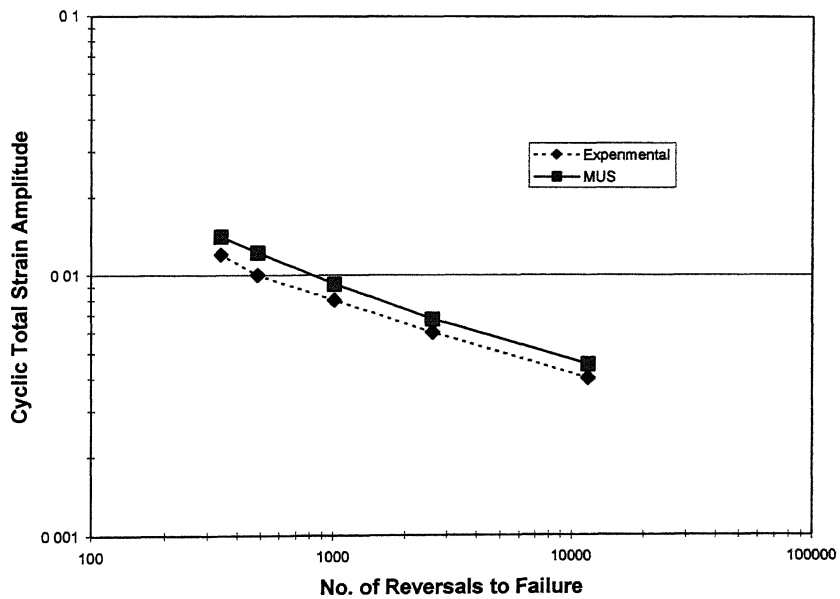


Figure 5.17 Cyclic total ,elastic and plastic strain amplitudesplotted as a function of number of load reversals to failure, $2N_f$. the intersection of elastic and plastic strain is the transition life $(2N_f)_t$ TMP1(PF/FP) condition.

(a)



(b)



(c)

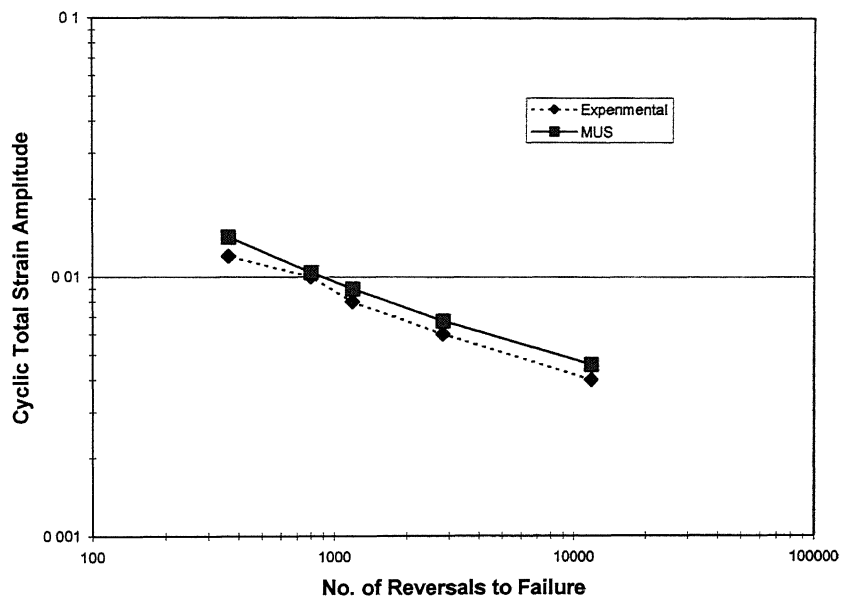
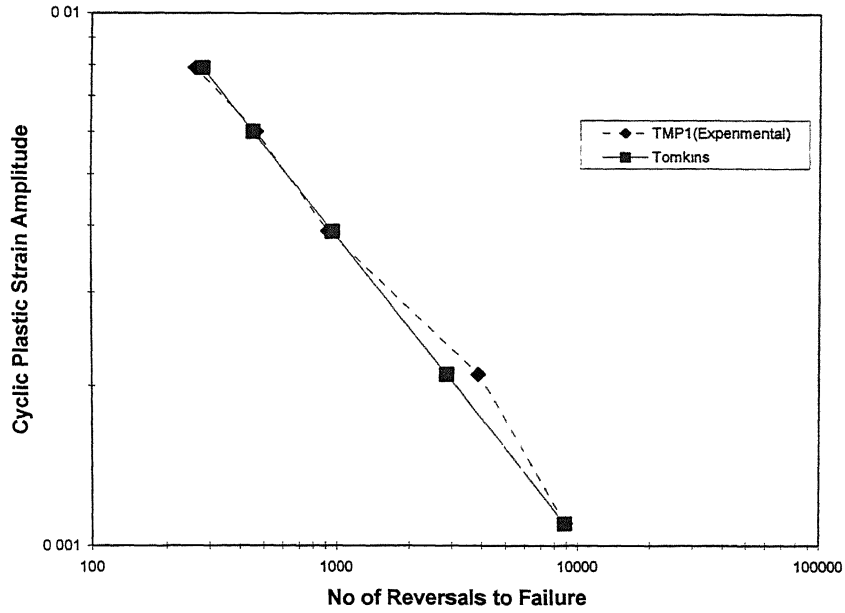
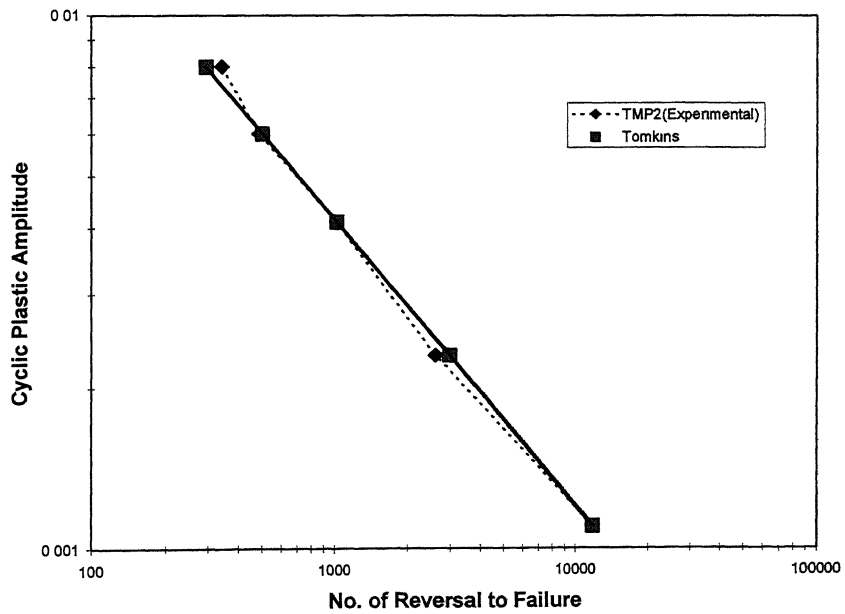


Figure 5.18 Life predicted by MUS model (a) TMP1 (PF/FP)(b) TMP2 (PF/MF)
(c) TMP3 (PF/CF)

(a)



(b)



(c)

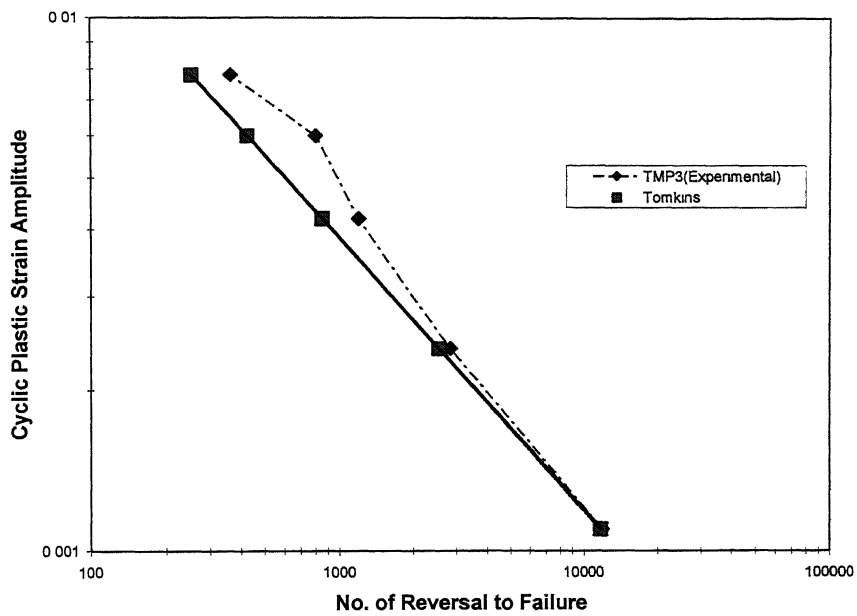


Figure 5.18 Life predicted by Tomkins' model (a) TMP1 (PF/FP) (b) TMP2 (PF/MF) (c) TMP3 (PF/CF)

exponent, c , for the PF/CP condition was greater than that for the PF/FP microstructure.

Similarly, a relation can be written for the elastic strain amplitude and this is called the Basquin relationship.

$$\frac{\Delta \varepsilon_e}{2} = \frac{\sigma'_f}{E} (2N_f)^b \quad (5.3)$$

where σ'_f is the fatigue strength coefficient and b is the fatigue strength exponent. The variation of elastic, plastic and total strain amplitudes for the TMP1(PF/FP) structure are plotted in Fig. 5.17 as function of the number of load reversals to failure, $2N_f$. The plot of strain and the number of reversals, besides providing useful quantitative information, offers a conceptual scheme for identifying the regimes wherein particular mechanisms and behavioral patterns are seen. These regimes are determined primarily by the relative levels of plastic and elastic strain. At high plastic strain, material ductility is the prime consideration governing the fatigue resistance. Cracks are found to initiate relatively early in the life and crack growth is the dominant failure mode. Conversely, at low plastic strain amplitudes, strength governs failure and crack initiation becomes the increasingly dominant event. The number of load reversals to failure $(2N_f)_t$, at which the elastic and plastic strains are equal is called the transition life [Suresh, 1991]. From Eqs. 5.2 and 5.3

$$(2N_f)_t = \left(\frac{\varepsilon'_f E}{\sigma'_f} \right)^{\frac{1}{b-c}} \quad (5.4)$$

Transition life for all the three structures is given in Table 5.6. At short fatigue lives, i.e., when $2N_f < (2N_f)_t$, the plastic strain amplitude is more dominant than the elastic strain amplitude and the fatigue life is controlled by ductility. At long fatigue lives, i.e., when $2N_f > (2N_f)_t$, the fatigue life is dictated by the rupture strength. Increasing strength increases long life resistance but decreases short life resistance, with an attendant decrease in the transition life. Thus, optimizing the overall fatigue properties inevitably requires a judicious balance between strength and ductility.

Table 5.6 Room temperature cyclic properties of material having three different microstructures

Condition	Cyclic Yield Stress	Cyclic Strength co-eff	Cyclic Strain hardening exponent	Fatigue ductility co-eff	Fatigue ductility exponent	Fatigue strength co-eff	Fatigue strength exponent	Transition life
	(CYS) MPa	K' (MPa)	n'	ϵ'_f	c	σ'_f (MPa)	b	$2(N_f)_t$ (cycles)
TMP-1 (PF/FP)	544	5512	0.37	0.16	-0.54	1407	-0.8	990
TMP-2 (PF/MP)	487	7061	0.43	0.19	-0.55	1470	-0.09	1200
TMP-3 (PF/CP)	439	8742	0.48	0.26	-0.58	1680	-0.11	1500

5.4.4 Fatigue Life Assessment

Attempts have been made to predict the fatigue life from the tensile data. One such empirical method, the modified universal slopes (MUS) method [Muralitharan and Manson, 1988] has been suggested to give reliable results. The MUS equation is given as

$$\Delta \epsilon_f = 1.17(\sigma_{UTS}/E)^{0.832} N_f^{-0.09} + 0.0266 \epsilon_f^{0.155} (\sigma_{UTS}/E)^{-0.53} N_f^{-0.56} \quad (5.5)$$

Tomkins (1968), using a phenomenological approach, has shown that

$$N_f = \frac{\ln\left(\frac{a_0}{a_f}\right)}{\left[\sec\left(\frac{\pi\sigma}{2\sigma_{UTS}}\right) - 1\right] \frac{\Delta\varepsilon_p}{2}} \quad (5.6)$$

Where a_0 and a_f are the initial and the final crack lengths respectively. The initial crack length is taken as $10\mu\text{m}$ and the final crack length is taken as $2/3$ diameter of the specimen, i.e. 6 mm [Tomkins, 1968]. Eqn. 5.6 can be reduced to

$$\frac{\Delta\varepsilon_p}{2} N_f^{1/(2n'+1)} = \text{constant} \quad (5.7)$$

by expanding the secant term and neglecting the higher order terms this form of the eqn. 5.6 (Eqn 5.7) is the same as the Coffin-Manson relationship and the exponent $c = -1/(2n'+1)$, where n' is the cyclic strain hardening exponent.

The experimental and predicted reversals to failure as per MUS and Tomkins' models are plotted in fig. 5.18 and fig. 5.19 respectively for all the three micro structural conditions. Both the models seen to fit experimental data reasonably well for all the microstructural conditions.

5.5 Effect of Thermomechanical Processing on High Cycle Fatigue Behavior

The stress-number of cycles to failure curves for the two structures (polygonal ferrite/fine pearlite and polygonal ferrite/medium pearlite) are shown in Fig. 5.20 (For better statistics, data from LCF tests were also included in the above plots). Tests were repeated at each stress level till two consistent results (within $\pm 20\%$) were obtained. Endurance limit was defined as the stress amplitude at which failure did not occur after 2×10^6 cycles. The data were fitted to a power law. Basquin relation (Eq. 5.3) was obeyed by all three structures. The parameters of the Basquin relation, σ'_f and b , correlation coefficient and endurance limit for the as-forged condition [Sarma, 1998] as well as the PF/FP, PF/MP structures studied in this investigation are given in Table 5.7. However, due to paucity of time the TMP3 condition was not studied in detail.

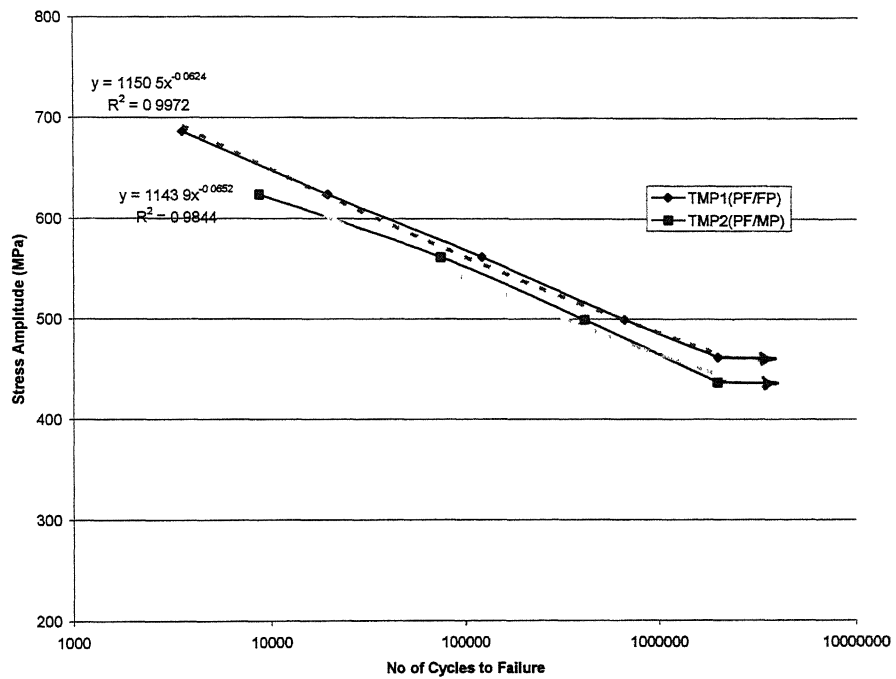


Figure 5.20 High Cycle Fatigue behavior of TMP1 & TMP2 conditions. The endurance limit is indicated by arrows.

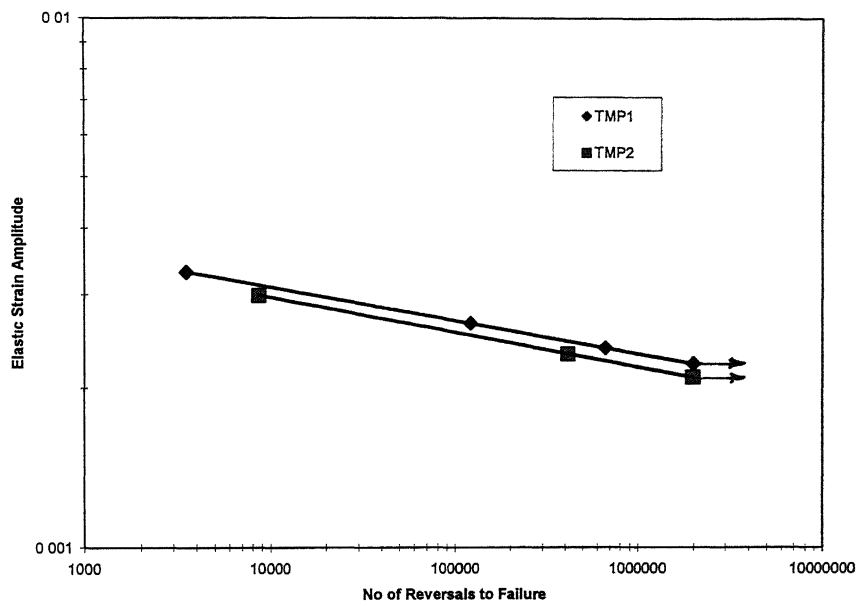


Figure 5.21 The elastic strain amplitude Vs No of reversals to failure ($2N_f$), TMP1 & TMP2 conditions.

Table 5.7 High cycle fatigue properties of 38MnSiVS5

Condition	σ'_f (MPa)	b	Correlation Coefficient	Endurance Limit (MPa)
As-Forged [Sarma, 1998]	1055	-0.08	-	320
TMP-1 (PF/FP)	1150	-0.06	0.99	462
TMP-2 (PF/MP)	1144	-0.06	0.98	437

From the above data we have,

$$\text{For TMP1 condition, } \Delta\epsilon_e/2 = 0.0055(2N_f)^{-0.0624} \quad (5.8)$$

$$\text{For TMP2 condition, } \Delta\epsilon_e/2 = 0.0054(2N_f)^{-0.0652} \quad (5.9)$$

These relations can be obtained by deviding the Basquin Eqn. by Young's Modulus E. The elastic strain amplitude Vs No. of reversals to failure ($2N_f$) plot for TMP1 and TMP2 are shown in fig. 5.21.

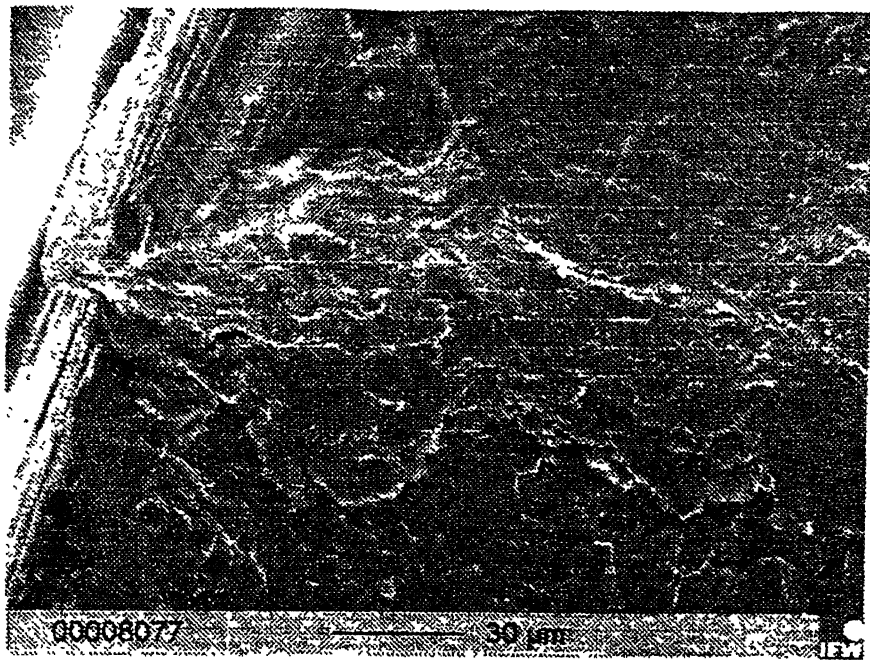
5.6 Fractography

Fracture surfaces of samples tested in the low cycle and high cycle fatigue regime were examined for sites of crack initiation and mode of crack propagation. The fractography was carried out on the tested samples of 49MnVS3 [Srivastava, 2000].

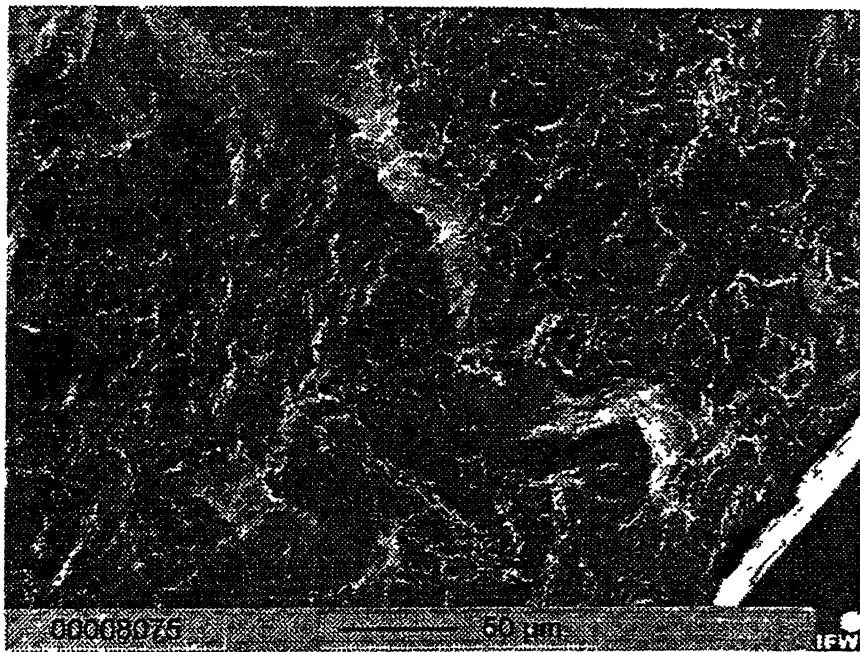
In polygonal ferrite/coarse pearlite, crack initiation took place predominantly near the surface at slip band extrusions/intrusions Fig. 5.22(a)[Srivastava, 2000]. Surface roughness and protrusions localize the stress and cyclic plastic strain, which leads to initiation of microcracks. In oxidizing atmosphere, rewelding is strongly inhibited by the oxidation of extrusion-intrusion surfaces [Hunsche and Neumann, 1988]. Stage I fatigue crack propagation at low as well as high plastic strain amplitude is observed in this condition near the surface Fig. 5.22(b)[Srivastava, 2000]. Stage II crack propagation takes place predominantly through microvoid growth and coalescence processes (Fig. 5.23a). Voids are generally observed to nucleate at inclusions and

precipitates where the interface between the matrix and the second phase particle is relatively weak. As seen from Fig. 5.23, the voids are of the order of 2-3 μm and do not correspond to the size of the inclusions, which are of the order of 50 μm . It has been shown that in the as-forged condition crack initiation does not commence from the inclusions even when they are present near the surface [Sarma, 1998]. This is because the more or less spherical/ellipsoidal MnS inclusions present play no part in crack nucleation under push-pull type of loading. This is the result of relatively lower modulus and high axial elongation present in the MnS inclusion. Consequently only low stress concentrations are present under push-pull type of loading [Eid and Thomason, 1979, Miller, 1993]. Void initiation, therefore, can be attributed to particle-matrix decohesion or cracking, depending on the relative strengths of the particle and the matrix. (This is in addition to the effect of the state of stress). Fine VC particles present in the steel are expected to be the void nucleating particles. Since the VC precipitate/matrix interface is incoherent and the VC precipitates are very hard, cracking of the VC precipitates is not expected. Void precipitates are very hard, cracking of the VC precipitates is not expected. Void growth can occur by plastic flow in the matrix or by a linkup of smaller voids that surround the large initial void. Crack growth by microvoid coalescence follows a zigzag pattern (as seen in Fig. 5.23a). The reason for this is that the plastic strain at crack tip is maximum at 45° to the macroscopic plane of crack growth. Striated crack growth, indicative of stage II fatigue crack growth, was also observed in Fig. 5.24.

In the polygonal ferrite/fine pearlite structure, the fracture behavior was similar to that for the PF/CP condition. Fatigue striations (Fig. 5.25a) indicate Stage II fatigue crack propagation. In many cases, uniformly spaced fatigue striations can be used to estimate the crack growth rate. Microvoid growth and coalescence was observed in this case as well (Fig. 5.25b). Shearing of inclusion is shown in fig. 26.



(a)



(b)

Figure 5.22 (a) Crack initiation at an intrusion on the surface in PF/CP material
(b) Stage I fatigue propagation in PF/CP material.

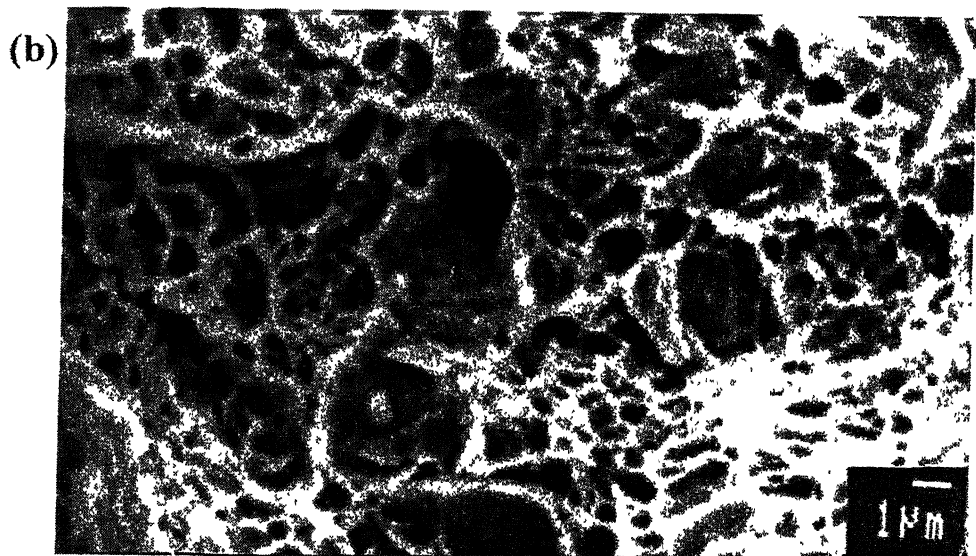
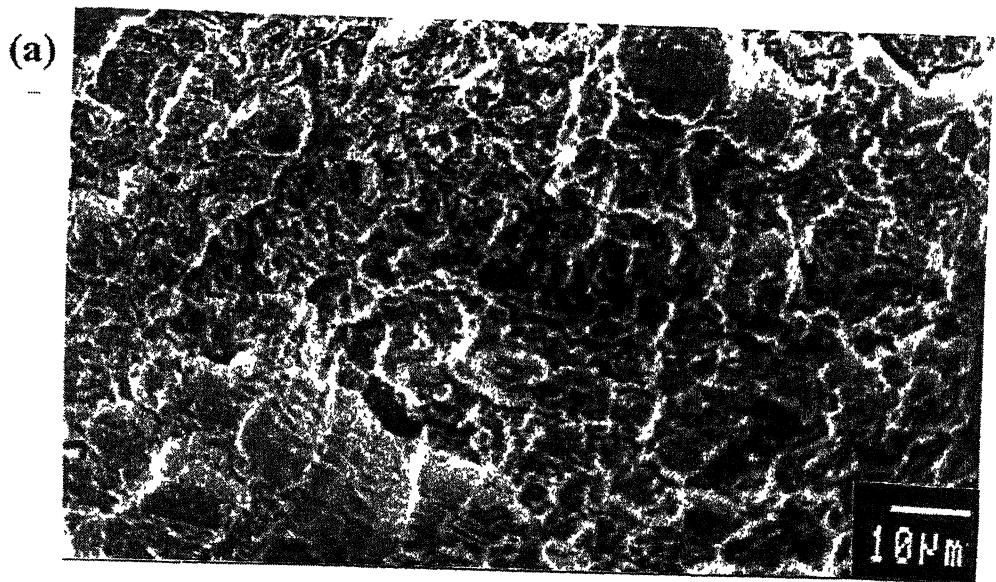


Figure 5.23 (a) Crack propagation by microvoid coalescence in PF/CP material.
(b) Enlarged view of (a)

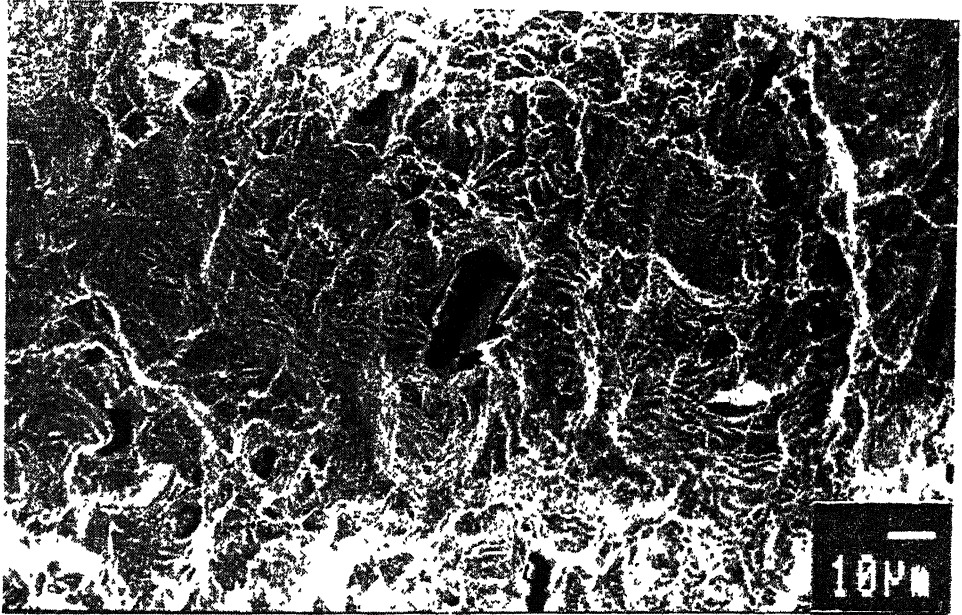


Figure 5.24 Striations associated with crack growth in PF/CP material.

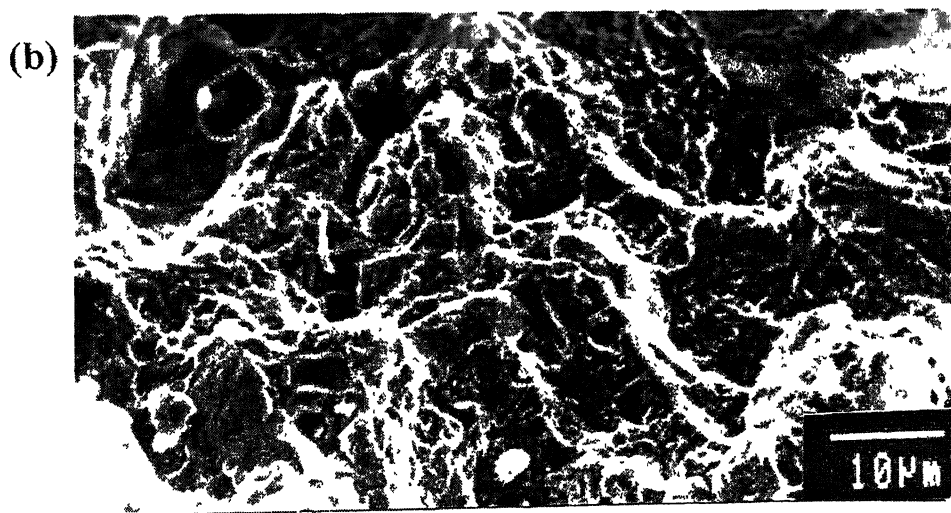
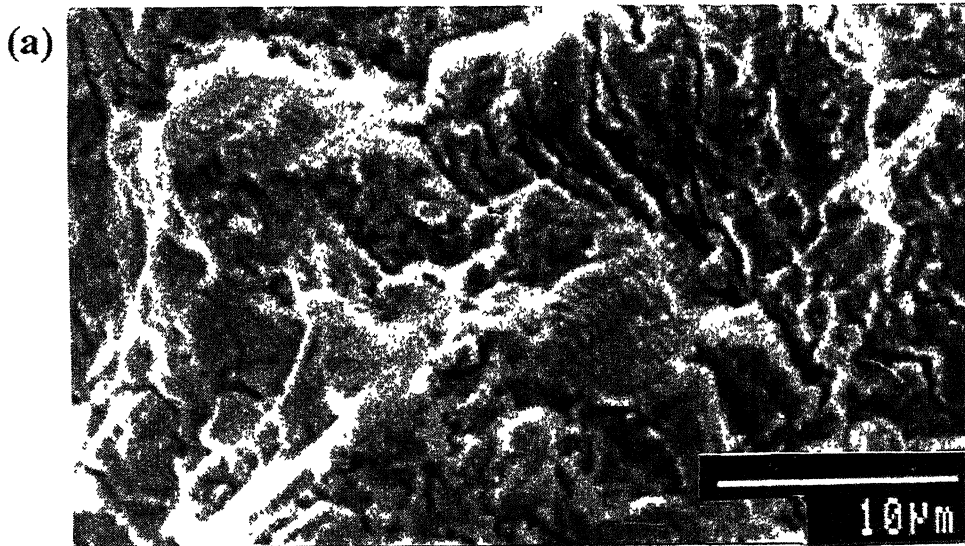


Figure 5.25 (a) Fatigue striations in PF/FP material.(b) Microvoid growth and coalescence in PF/FP material.

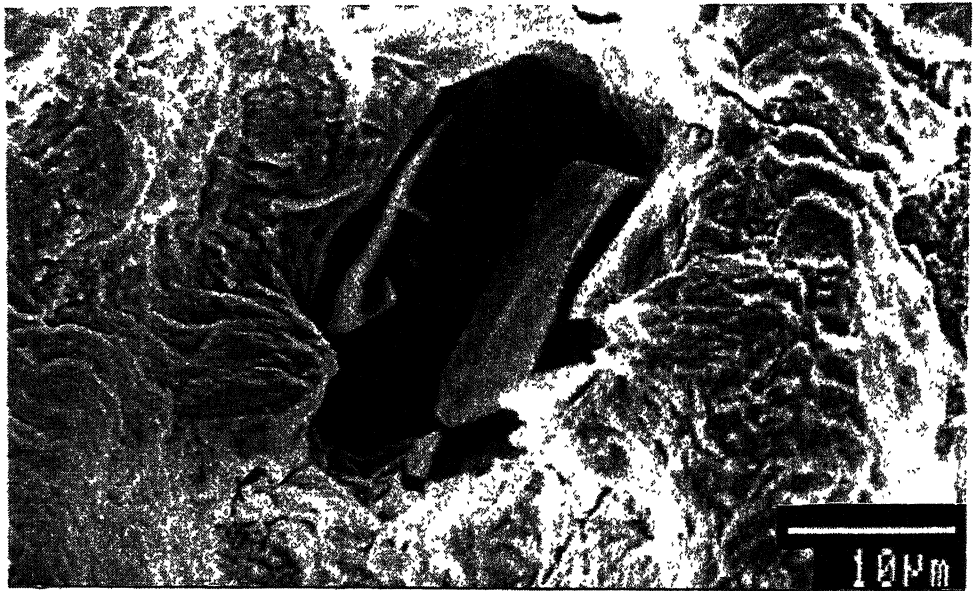


Figure 5.26 Shearing of Inclusion.

Conclusions and Suggestions for Future Work

6.1 Conclusions

Some major conclusions that have resulted from the present investigation are

1. Thermo-mechanical processing at 800°C, 900°C & 1000°C (i.e. finish rolling temperature followed by air cooling) resulted in a polygonal ferrite/fine pearlite, polygonal ferrite/medium pearlite and polygonal ferrite/coarse pearlite microstructures respectively.
2. Best combination of monotonic strength and ductility was obtained in a polygonal ferrite/fine pearlite microstructure. The tensile strength in this condition was 15% more than that for the as-received material.
3. In all the microstructures, at total strain amplitudes in the range of 0.4-0.6% cyclic softening in the first few cycles was followed by steady-state behavior. At greater total strain amplitudes than 0.6 cyclic hardening was observed. However, the degree of hardness was most for TMP3 condition.
4. Cyclic yield strength was found to be maximum for the polygonal ferrite/fine pearlite microstructure.
5. In the low cycle fatigue regime, the fatigue life for the polygonal ferrite/coarse pearlite microstructure exceeded that of the polygonal ferrite/fine pearlite microstructure by nearly 35% to 60% at low plastic strain amplitude (0.11 to 0.39%) and high plastic strain amplitude (0.40 to 0.80%) respectively. However, on total strain amplitude basis the fatigue lives were nearly the same for all the three microstructures.
6. Fatigue crack propagation in both the polygonal ferrite/coarse pearlite and polygonal ferrite/fine pearlite microstructures was by micro-void growth.

7. Fatigue life in stress controlled, high cycle fatigue regime was found to be the greatest for the polygonal ferrite/fine pearlite microstructure. The fatigue limit in this condition was estimated to be 462 MPa.

6.2 Suggestions for Future Work

1. Temperature range for the thermomechanical processing should be widened. Two step cooling process should also be investigated.
2. Particle size and distribution of precipitates in the matrix should be studied and quantified. Effort should be made to estimate the amount of strengthening obtained by precipitation hardening in this microalloyed steel.
3. Transmission electron microscopy should be used to understand the mechanism(s) of fatigue crack initiation and damage evolution.
4. Fracture toughness measurements should be undertaken and the fracture mechanics approach to fatigue investigated.
5. The influence of the orientation of the inclusions on the fatigue behavior can be investigated.
6. Effect of stress ratio, R , and a non-zero mean stress should be studied.
7. The growth of short cracks can be studied. Crack threshold and crack propagation studies in the Paris' regime should be undertaken.
8. Cumulative damage under and variable amplitude loading should be studied.

references

1. Amin, R.K., Pickering, F.B. (1982), in: *Thermo-mechanical Processing of Microalloyed Austenite*: De Ardo, A.J., Ratz, G.A., Wray, P.J. (Eds.). Warrendale PA: AIME, p.1
2. Ashby, M.F. (1966), *Phil. Mag.* **14**, 1157
3. Ballinger, N.K., Gladman, T. (1979), *Met. Science* **15**, 95
4. Bhambri, S. K., Prasad, C. R., Vasudevan, R. (1989), *Int. J. Fatigue* **7**, 239
5. Blarasin, A., Faretti, P. (1989), *Int. J. Fatigue* **11** (1), 13
6. Brown, L. M., Stobbs, M. M. (1971), *Phil. Mag.* **23**, 1185
7. Coldren, A P., Tither, G. (1978), *J. Metals* **30** (4), 6\
8. Cooke, R.J., Beevers, C.J. (1974), *Mat. Science Engg.* **13**, 201
9. Cracknell, A., Petch, N. J. (1955), *Acta. Met.* **3**, 186
10. Davies, R G. (1978), *Met. Trans.* **9A**, 41, 451 and 671
11. Dinda, G.P. (2001), M.Tech Thesis, Indian Institute of Technology, Kanpur
12. Dollar, M. Bernstein, J. M., Daeubler M., Thompson, A W. (1989), *Met. Trans.* **20A**, 447
13. Dollar, M. Bernstein, J. M., Thompson, A. W. (1988), *Acta. Metall.* **36**, 311
14. Duckworth, W. E. (1965), *J. Iron Steel Inst. London* **204**, 1108
15. Eid, N. M. A. and Thomason, P. F. (1979), *Acta. Metall.* **27**, 1239
16. Farrar, 1. C. M. (1971), in: *Effect of Second Phase Particles on the Mechanical Properties of Steels*. London: The Iron and Steel Institute, p. 171

17. Farsetti, I(Blarasin, A (1988),*Int. J Fatigue* 10, 153
18. Fix, R. M., Zheng, Y. Z., De Ardo, A.J. (1986), in: *HSLA Steels- Metallurgy and Applications*: Gray, J. M. et.al. (Eds.). Metals Park, OH: ASM International, p. 219
19. Gladman, T., Dulieu, D., McIvor, J. D. (1977), in: *Microalloying* 75: Korchynsky, M (Ed.). New York: Union Carbide Corporation, p.25
20. Gladman, T., Pickering F. B. (1967), *J. Iron Steel Inst. London* 205, 653\
21. Gladman, T., Pickering F. B. (1983), in: *Yield, Flow and Fracture of Polycrystals*: Baker, T.N. (Ed.). London: Applied Science Publishers, p. 141
22. Gray, III G. T., Thompson, A. W., Williams, J. C. (1985), *Met. Trans.* 16A,753
23. Hilty, D. C., Popp, V. T. (1969), *Electric Furnace Conference Proceedings*, AIME, 27, 52.
24. Honeycombe, R. W. K. (1986), in: *HSLA Steels- Metallurgy and Applications*: Gray, J. M. et. al. (Eds.). Metals Park, OH: ASM International, p. 243
25. Hunsche, A. and Neumann, P. (1988), *Basic Questions in Fatigue* 1,26
26. Irvine, K. J., Gladman, T., Pickering, F. B. (1970), *J. Iron Steel Inst. London* 208, 717\
27. Kim, Y. H., Fine, M. E. (1982), *Met. Trans.* 13A, 80\
28. Korchynsky, M., Stuart, H. (1970), in: *Low Alloy High Strength Steels*. Nurnberg: Metallurg, p.17
29. Korchynsky, M. (1990), in: *Microalloyed Vanadium Steels*: Korchynsky, M. et.al. (Eds.). Krakow: Association of Polish Metallurgical Engineers and Strategic Minerals Corp., p. 5

30. Lanzillotto, C. A. N., Pickering, F. B. (1982), *Met. Science* 16,371
31. Little, J. H., Henderson, W. L. M. (1971), in: *Effect of Second Phase Particles on the Mechanical Properties of Steels*. London: The Iron and Steel Institute, p.182
32. Liu, C. D., Bassim, M. N., Lawrence, S. St. (1993), *Mat. Science Engg.* A167, 107
33. Lucas, J. P., Gerberich, W. W. (1985), *Int. J. Fatigue* 7,31
34. Matsuda, S., Okumura, N, (1978), *Trans. Iron Steel Inst. Japan* 18, 198
35. Mediratta, S. R., Ramaswamy, V. and Raffia Rao, P. (1985), *Int. J. Fatigue* 7,101
36. Metals Handbook (1990) 1, Davies, J. R. et.al. (Eds.). Metals Park, OH: ASM, p 389-422
37. Meyer, L., Heisterkamp, F., Mueschenborn, W. (1977), in: *Microalloying 75*: Korchynsky, M. (Ed). New York: Union Carbide Corporation, p153
38. Meyer Lutz, Wolfgang Muschenborn and Schrieffer .Thermo-Mechanical Processing in Theory,Modelling & Practice [TMP]² Editors B.Hutchinson,M.Andersson,G.Engberg,B.Karlson,T.Siwecki (Page No. 97-100).
39. Michelich, J. H., Bell, J. R, Korchynsky, M. (1971), *J. Iron Steel Inst. London* 209, 469
40. Miller, K. J. (1993),*Mat. Sc: Tech.* 9,453
41. Muralitharan, U. and Manson, S.S. (1988) *J: Engg. Mater. Teck* 110,55
42. Narita, K. (1975), *Trans. Iron Steel Inst. Japan*, 15,145
43. Owen, W. S. (1980),*Metals Technology* 7 (1),1

44. Petch, N. J. (1953), *J. Iron Steel Inst. London* 174, 25
45. Phillips, R., Chapman, J. A (1966), *J. Iron Steel Inst. London* 204,615
46. Pickering, F. B. (1992) in: *MST7*: Pickering, F. B. (Ed.). New York: VCH, p339- 394
47. Plumbridge, W. J., Bartlett, R. A. (1982), *Int. J. Fatigue* 4,209
48. Poh1, K., Mayr, P., Macherauch, E. (1981), *Int. J. Fracture* 17,773
49. Porter, L.F. (1986), in: *Encyclopedia of Materials Science and Engineering*. 3, Pennagon Press and MIT Press, p. 2157
50. Roberts, w. (1984), in: *HSLA Steels- Technology and Applications*. Korchynsky, M. (Ed.). Metals Park, OH:ASM, p33
51. Roberts, W., Sandberg, A, Siweck, T., Werlefors, T. (1984), in: *HSLA Steels- , Technology and Applications*, :Korchynsky, M. (Ed.). Metals Park, OH:ASM, p67
52. Robert, W., Sandberg, A. (1985), *Report No. M-1489*. Stockholm: Swedish Institute for Metals Research
53. Roven, H. J. and Res, E. (1991), *Acta. Metal/. Mater.* 39, 1735
54. Santner, J.S. andFine, M. E. (1977), *ScriptaMet* 11, 159 J
55. Sarma, V.S., SunderaRaman, M. and Padmanabhan, K. A (1998), *Mat. Sc. Tech* 14, 669
56. Sarma, V. S (1998), *Ph. D. Thesis*, Indian Institute ofTechnology, Madras
57. Sigalla, A (1957), *.I Iron Steel Inst. London* 186,90
58. Singh, H., Raju, P. V. S. S., Namboodhiri, T. K. G., Rama Rao, P. (1990), *Int. J. Fatigue* 12, 289

59. Singh, V., SundaraRaman, M., Chen, Ww. and Wahi, R. P. (1991), *Met. Trans.* 22A, 499
60. Srivastava, V (2000), M.Tech. Thesis, Indian Institute of Technology, Kanpur.
61. Sunwoo, H., Fine, M. E., Meshii, M., Stone, D. H. (1982), *Met. Trans.* 13A, 2035
62. Suresh, S. (1991), *Fatigue of Materials*. London: Cambridge
63. Tamura, J., Ouchi, C., Tanaka, T., Sekine, H. (1988), *Thermo-mechanical Treatment*
64. *Processing of High Strength Low Alloy Steels*. London: Butterworth 61.
Tanaka, T. (1981), *Int. Met. Reviews* 1981 (4), 185
65. Tanaka, T., Tabata, N., Hatomura, T, Shiga, C. (1977), in: *Microalloying 75*: Korchynsky, M. (Ed.). New York: Union Carbide Corporation, p88
66. Thompson, S. W., Krauss, G. (1989), *Met. Trans.* 20A, 2279
67. Tomkins, B. (1968), *Phil. Mag.* 18, 1041
68. Weister, H.I., Ulmer, H. (1959), *Stahl u. Eisen* 79, 1120
69. Williams, D. B., Newbury, D. E., Goldstein, I. J., Fiori, C. E. (1984), *J. Microscopy* 136, 209
70. Wrigth, P.H. (1990), in: *Metals Handbook*. I, Davies, I. R. et al. (Eds.). Metals Park, OH: ASM, p358
71. Xiao-Yan, T., De-lun, W. and Hao, X. (1989), *Int. J. Fatigue* 11, 353
72. Yang, L., Fatemi, A (1995), *J. Testing Evaluation* 23, 80

73. Zajac, S.t Siweckit T., Hutchinson, B., Attlegard, M. (1990), -In: *Microalloyed Vanadium Steels*: Korchynsky, M. et. al. (Eds.). Krakow: Association of Polish Metallurgical Engineers and Strategic Minerals Corp., p. 149
74. Zheng, Y. Z., Fitzsimons, G, De Ardo, A. J. (1984), in: *HSLA Steels-Technology and Applications*, Korchynsky, M. (Ed.). Metals Park, OH:ASM, p85

A137952



A137952